



**UNIVERSITY OF LEEDS**

This is a repository copy of *Seven indicators variations for multiple PV array configurations under partial shading and faulty PV conditions*.

White Rose Research Online URL for this paper:  
<http://eprints.whiterose.ac.uk/117259/>

Version: Accepted Version

---

**Article:**

Dhimish, M, Holmes, V, Mehrdadi, B et al. (3 more authors) (2017) Seven indicators variations for multiple PV array configurations under partial shading and faulty PV conditions. *Renewable Energy*, 113. pp. 438-460. ISSN 0960-1481

<https://doi.org/10.1016/j.renene.2017.06.014>

---

© 2017 Elsevier Ltd. This manuscript version is made available under the CC-BY-NC-ND 4.0 license <http://creativecommons.org/licenses/by-nc-nd/4.0/>

**Reuse**

Items deposited in White Rose Research Online are protected by copyright, with all rights reserved unless indicated otherwise. They may be downloaded and/or printed for private study, or other acts as permitted by national copyright laws. The publisher or other rights holders may allow further reproduction and re-use of the full text version. This is indicated by the licence information on the White Rose Research Online record for the item.

**Takedown**

If you consider content in White Rose Research Online to be in breach of UK law, please notify us by emailing [eprints@whiterose.ac.uk](mailto:eprints@whiterose.ac.uk) including the URL of the record and the reason for the withdrawal request.

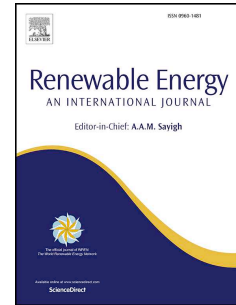


[eprints@whiterose.ac.uk](mailto:eprints@whiterose.ac.uk)  
<https://eprints.whiterose.ac.uk/>

# Accepted Manuscript

Seven indicators variations for multiple PV array configurations under partial shading and faulty PV conditions

Mahmoud Dhimish, Violeta Holmes, Bruce Mehrdadi, Mark Dales, Benjamin Chong, Li Zhang



PII: S0960-1481(17)30515-3

DOI: [10.1016/j.renene.2017.06.014](https://doi.org/10.1016/j.renene.2017.06.014)

Reference: RENE 8878

To appear in: *Renewable Energy*

Received Date: 20 March 2017

Revised Date: 2 May 2017

Accepted Date: 1 June 2017

Please cite this article as: Dhimish M, Holmes V, Mehrdadi B, Dales M, Chong B, Zhang L, Seven indicators variations for multiple PV array configurations under partial shading and faulty PV conditions, *Renewable Energy* (2017), doi: 10.1016/j.renene.2017.06.014.

This is a PDF file of an unedited manuscript that has been accepted for publication. As a service to our customers we are providing this early version of the manuscript. The manuscript will undergo copyediting, typesetting, and review of the resulting proof before it is published in its final form. Please note that during the production process errors may be discovered which could affect the content, and all legal disclaimers that apply to the journal pertain.

# Seven indicators variations for multiple PV array configurations under partial shading and faulty PV conditions

Mahmoud Dhimish<sup>1</sup>, Violeta Holmes<sup>1</sup>, Bruce Mehrdadi<sup>1</sup>, Mark Dales<sup>1</sup>, Benjamin Chong<sup>2</sup>, Li Zhang<sup>2</sup>

<sup>1</sup> School of Computing and Engineering, University of Huddersfield, United Kingdom

<sup>2</sup> School of Electronic and Electrical Engineering, University of Leeds, United Kingdom

## Abstract

The goal of this paper is to model, compare and analyze the performance of multiple photovoltaic (PV) array configurations under various partial shading and faulty PV conditions. For this purpose, a multiple PV array configurations including series (S), parallel (P), series-parallel (SP), total-cross-tied (TCT) and bridge-linked (BL) are carried out under several partial shading conditions such as, increase or decrease in the partial shading on a row of PV modules and increase or decrease in the partial shading on a column of PV modules. Additionally, in order to test the performance of each PV configuration under faulty PV conditions, from 1 to 6 Faulty PV modules have been disconnected in each PV array configuration. Several indicators such as short circuit current ( $I_{sc}$ ), current at maximum power point ( $I_{mpp}$ ), open circuit voltage ( $V_{oc}$ ), voltage at maximum power point ( $V_{mpp}$ ), series resistance ( $R_s$ ), fill factor (FF) and thermal voltage ( $V_{te}$ ) have been used to compare the obtained results from each partial shading and PV faulty condition applied to the PV system. MATLAB/Simulink software is used to perform the simulation and the analysis for each examined PV array configuration.

**Keywords:** Multiple PV array configurations, Partial shading, Fault detection, MATLAB/Simulink

## 1. Introduction

Growing interest in renewable energy resources has caused the photovoltaic (PV) power market to expand rapidly. The power produced by grid-connected photovoltaic (GCPV) plants depends on various conditions such as PV module's temperature and irradiance level. Shading by the surroundings directly effects both the cell temperature and irradiance level incident on the GCPV systems [1]. There are multiple reasons for the shading affects GCPV systems. K. Lappalainen & S. Valkealahti [2] discussed the output power variations of different PV array configurations during irradiance transition caused by moving cloud. The results shows that the average rate of change in the output power during irradiance transitions is around 3%, where the maximum rate of change is approximate to 75%. Furthermore, an accurate approach method to simulate the characteristics output of a PV systems under either partial shading or mismatch conditions is proposed by J. Bai et al [3]. The method is using the analysis of the current-voltage (I-V) and power-voltage (P-V) curves for various PV systems.

A highly detailed PV array model is developed by M. Vincenzo et al [4], the PV model was developed under non-uniform irradiance conditions using PSpice. The model assumed that the PV cells temperature are homogenous for each PV module which makes the simulation and modelling of the PV system less complex. The output results shows a good agreement between the simulation model vs. outdoor experimental results. The losses associated to shading effect can be reduced by using several approaches such as the maximum power point tracking (MPPT) techniques that allow the extension of the global maximum power point. R. Yeung et al [5] proposed a global MPPT algorithm which is based on extracting the power-voltage characteristics of the PV string through varying the input power impedance.

42 PV array configurations which is considered in this paper is one of solutions that can significantly reduce  
43 mismatch and shading losses in GCPV plants. It is based on the PV array interconnections of PV modules  
44 which are series (S), parallel (P), series-parallel (SP), total-cross-tied (TCT) and bridge-linked (BL) and  
45 many other configurations. Several attempts were proposed by researchers to study and analyze the effect  
46 of shading on different PV array configuration in order to reduce mismatch losses and providing the  
47 maximum output power generation. These attempts can be illustrated by the following:

48 1. Comparison of various PV array configurations:

49 F. Belhachat & C. Larbes [6] detailed a brief comparison between five different PV array  
50 configurations (S, P, SP, TCT and BL configurations). The analysis is based on  
51 MATLAB/Simulink software. The results prove that TCT configuration achieved the optimum  
52 output power performance under most shading conditions. Moreover, [7] shows a mathematical  
53 analysis of TCT PV array configuration under partial shading conditions and its comparison with  
54 other PV array configurations such as BL and honey-comb (HC) configurations. Y. Wang & P.  
55 Hsu [8] found again that in most cases TCT configuration has a superior performance over the  
56 other PV array configurations such as S, P and SP. Some other publications are based on a  
57 comprehensive review on PV array configuration under partial shading conditions such as [9 &  
58 10].

59  
60 2. New proposed PV array configuration:

61 S. Pareek & R. dahiya [11] proposed a new method that allows the distribution of shading effect  
62 evenly in each PV row thereby enhance the PV array output power. The PV characteristics curves  
63 for the proposed method is much smoother than other PV array configurations such as TCT.  
64 Furthermore, B. Rani et al [12] suggested a new method for increasing the power generation from  
65 PV array configuration. In the proposed approach, the physical location of the PV modules are  
66 connected using TCT configuration, but all PV arrays are arranged based on “Su Do Ku” puzzle  
67 pattern. The performance of the system is investigated for different shading patterns and the  
68 results show that positioning the modules of the array according to “Su Do Ku” puzzle pattern  
69 yields improved performance under partially shaded conditions. However, this method faces a  
70 drawbacks due to ineffective dispersion of shade and significant increase in wiring requirements,  
71 these disadvantages of the “Su Do Ku” method have been enhanced using a new technique which  
72 is proposed by S. Potnure et al [13].

73  
74 3. Power electronics techniques for enhancing PV power generation:

75 B. Chong & L. Zhang [14] proposed a new controller design for integrated PV-converter modules  
76 under partial shading conditions. The control results showing rapid and stable responses are  
77 superior to that obtained by bypass diode structure which is conventionally controlled using  
78 perturbation-and-observation method. Furthermore, a new GCPV based on cascaded H-Bridge  
79 quasi-z source inverter is presented by [15], the technique is used to verify the multilevel PV  
80 interface with AC inverters to enhance the power generation of GCPV systems. E. Koutroulis &  
81 F. Blaabjerg [16] proposed a new procedure for tracking the global maximum power point of PV  
82 arrays operating under partial shading conditions using D-flip/flop and analog/digital converter  
83 strategy. Additionally, a brief comprehensive maximum power point extraction using genetic  
84 algorithm is shown in [17].

85  
86 4. PV fault detection algorithms:

87 There are various methods used to detect faults in GCPV plants. Some of these methods use  
 88 statistical analysis techniques such as t-test [18 & 19] and standard deviation limits [20].  
 89 Furthermore, machine learning techniques have been also applied in PV systems for fault  
 90 detection purposes. ANN network was used by [21] for detection multiple faults in a PV system  
 91 such as faulty PV modules and faulty bypass diodes. S. Silvestre et al [22] proposed a new  
 92 procedure for fault detection in PV systems which is based on the analysis of the voltage and  
 93 current ratios for the entire GCPV plant.

94 In this work, we present a detailed modelling, comparison and data analysis for multiple PV array  
 95 configurations including the series (S), parallel (P), series-parallel (SP), total-cross-tied (TCT) and bridge-  
 96 linked (BL) configurations. In order to compare the performance for each PV array configuration, various  
 97 partial shading and faulty PV conditions have been tested. Several indicators such as short circuit current  
 98 ( $I_{sc}$ ), current at maximum power point ( $I_{mpp}$ ), open circuit voltage ( $V_{oc}$ ), voltage at maximum power point  
 99 ( $V_{mpp}$ ), series resistance ( $R_s$ ), fill factor (FF) and thermal voltage ( $V_{te}$ ) have been used to compare the  
 100 obtained by the tested partial shading and faulty conditions.

101 Fig. 1 shows the overall examined PV array configurations, tested case scenarios and all indicators used  
 102 to compare the performance between each PV array configuration. As can be noticed, the partial shading  
 103 conditions applied in this paper is not static, which means that the partial shading conditions are either  
 104 increasing or decreasing among all PV modules. Additionally, in order to test the performance of each PV  
 105 array configuration under faulty PV conditions, from 1 to 6 Faulty PV modules have been disconnected in  
 106 order to compare between each PV indicator variations.

107 From the literature, there is a few data analysis on the indicators variations among partial shading and  
 108 faulty PV conditions applied to multiple PV array configurations, therefore, the main contribution of this  
 109 article is the comparison and data analysis of multiple PV array configurations using seven different  
 110 indicators. The examined indicators has not been fully covered in previously published articles such as [6-  
 111 10]. Additionally, this research does not only examine several partial shading conditions affecting PV  
 112 systems but also the modelling and the analysis of several faulty PV conditions (In-active PV modules)  
 113 affecting various PV array configurations.

114 This paper is organized as follows: Section 2 presents the modelling and simulation for one PV module  
 115 using MATLAB/Simulink software. Section 3 describes the calculation of the diagnostic indicators, while

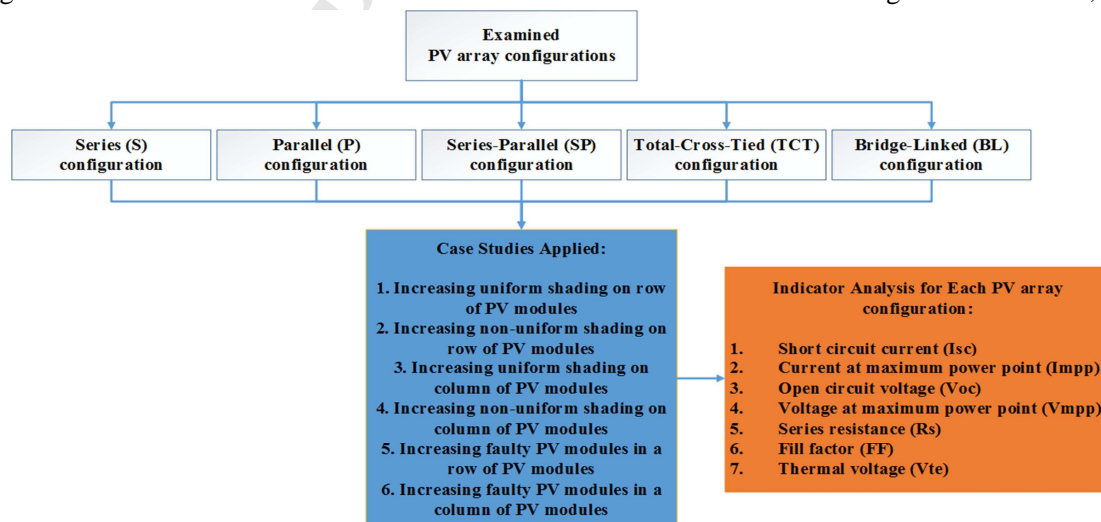


Fig. 1. All Listed PV Array Configurations Compared in this Paper, Tested Case Studies and All Indicators Used to Compare the Performance of Each PV Array Configuration

116 section 4 illustrates the simulation, modelling and data analysis of the examined PV array configurations.  
 117 Finally, section 5 and section 6 describes the discussion and the conclusion respectively.

## 118 2. Modelling and simulation of one PV module

119 In this work, MATLAB/Simulink software is used to model, simulate and analyze the performance of the  
 120 examined PV modules. Fig. 3(a) shows the equivalent circuit of a PV module. The voltage and the current  
 121 characteristics of the PV module can be obtained using the single diode model [23] as explained in (1).

$$122 \quad I = I_{ph} - I_o \left( e^{\frac{V+IR_s}{N_s V_t}} - 1 \right) - \frac{V+IR_s}{R_{sh}} \quad (1)$$

123 where  $I_{ph}$  is the photo-generated current at STC,  $I_o$  is the dark saturation current at STC,  $R_s$  is the  
 124 module series resistance,  $R_{sh}$  is the panel parallel resistance,  $N_s$  is the number of series cells in the PV  
 125 module and  $V_t$  is the thermal voltage and it can be calculated using (2).

$$126 \quad V_t = \frac{A k T}{q} \quad (2)$$

127 where  $A$  the diode ideality factor,  $k$  is Boltzmann's constant,  $T$  is the module temperature in kelvin and  $q$   
 128 is the charge of the electron.

129 The five parameters model are determined by solving the transcendental equation (1) using Newton-  
 130 Raphson algorithm [24] based only on the datasheet of the available parameters shown in Table I. The  
 131 power produced by PV module in watts can be easily calculated along with the current ( $I$ ) and voltage ( $V$ )  
 132 that is generated by equation (1), therefore,  $P_{\text{theoretical}} = IV$ .

133 Fig 3(b) shows the PV module simulated at standard test conditions (STC):

- 134 • Irradiance  $1000 \text{ W/m}^2$ , spectrum AM 1.5 G
- 135 • PV module temperature  $25 \text{ }^\circ\text{C}$

136 Using the MATLAB/Simulink software, it is possible to simulate the output voltage, current and the  
 137 power of the PV module as shown in Fig. 3(c). As an example of simulation, Fig 2(a) and Fig2(b) show  
 138 respectively the I-V and P-V curves of one PV module of 60 solar cells obtained with Simulink using the

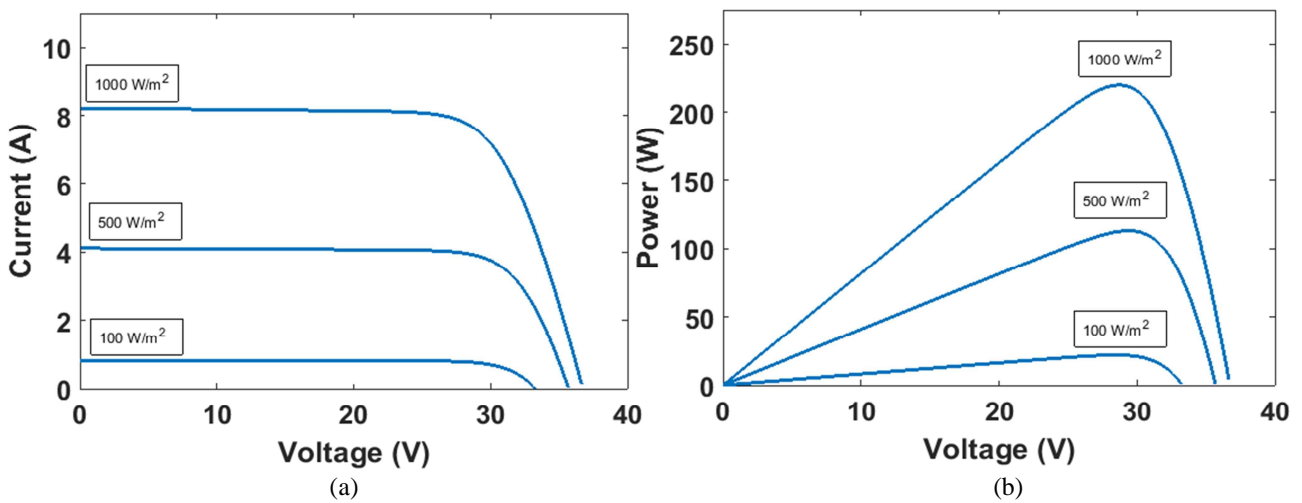


Fig. 2. Simulation Results of MATLAB/Simulink model. (a) Photovoltaic I-V Curve, (b) Photovoltaic P-V Curve

139 model described in Fig. 3(c). In this paper, the solar cell parameters used in the simulation are shown in  
140 Table1.

ACCEPTED MANUSCRIPT

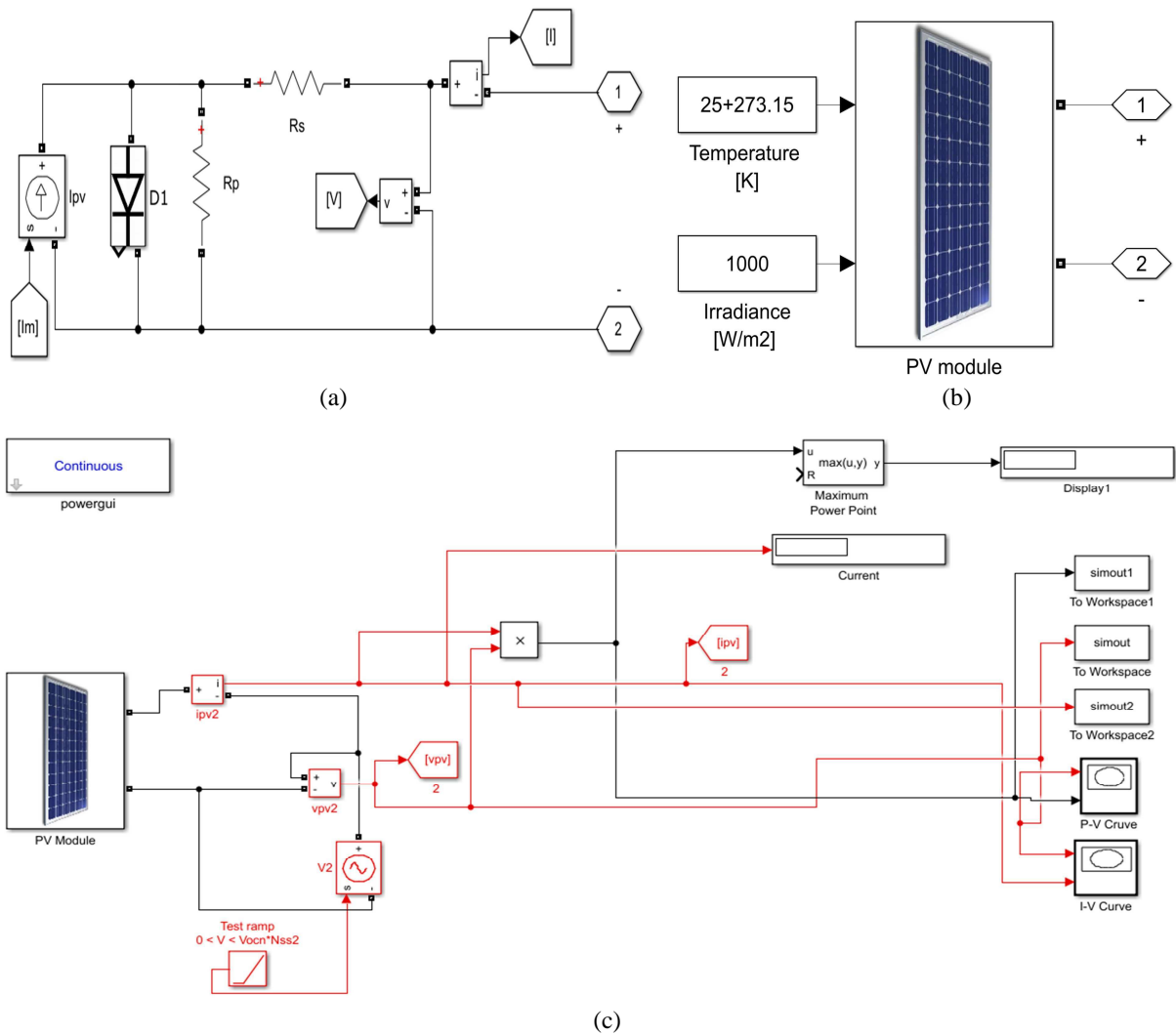


Fig. 3. Photovoltaic Modelling Using MATLAB/Simulink. (a) Equivalent Circuit of a Solar Module, (b) Simulating PV Module under STC, (c) Simulating the Output Voltage, Current and Power of the PV Module

Solar panel electrical characteristics	Value
Peak power	220 W
Voltage at maximum power point ( $V_{mp}$ )	28.7 V
Current at maximum power point ( $I_{mp}$ )	7.67 A
Open circuit voltage ( $V_{oc}$ )	36.74 V
Short circuit current ( $I_{sc}$ )	8.24 A
Number of cells connected in series	60
Number of cells connected in parallel	1
Series resistance ( $R_s$ )	0.48484 $\Omega$
Parallel resistance ( $R_{sh}$ )	258.75 $\Omega$
Dark saturation current ( $I_o$ )	$2.8 \times 10^{-10}$ A
Ideal diode factor (A)	0.9117
Boltzmann's constant (k)	$1.3806 \times 10^{-23}$ J.K <sup>-1</sup>

### 141 3. Calculation of the diagnostic indicators

142 In order to compare the behavior of various PV array configurations. Firstly, it is required to identify the  
 143 main indicators needed to investigate the change of the PV array configurations behavior. In this paper, a  
 144 comparison between  $V_{mpp}$ ,  $V_{oc}$ ,  $I_{mpp}$ ,  $I_{sc}$  and  $P_{mpp}$  have been estimated for various PV array configurations.  
 145 Additionally, new diagnostic indicators have been used and briefly explained in this section.

#### 146 3.1 Equivalent thermal voltage ( $V_{te}$ )

147 In previous work [25 & 27] an estimation of the thermal voltage of a PV model under partial shading  
 148 conditions has been expressed by (3).

$$149 \quad V_{te} = \frac{(2V_{mp} - V_{oc})(I_{sc} - I_{mp})}{I_{mp} - (I_{sc} - I_{mp}) \ln\left(\frac{I_{sc} - I_{mp}}{I_{sc}}\right)} \quad (3)$$

150 where  $V_{mp}$  is voltage at maximum power point,  $I_{mp}$  presents the current at the maximum power point,  $V_{oc}$   
 151 is the open circuit voltage and  $I_{sc}$  is the short circuit current estimated by the I-V or P-V curve of the PV  
 152 module.

153 A second commonly used method to estimate the thermal voltage is to evaluate the change of the diode  
 154 ideality factor  $A$  of the PV module [26]. This method can be calculated using (4).

$$155 \quad V_{te} = \frac{N_s A k T}{q} \quad (4)$$

156 where  $N_s$  is the number of solar cells connected in series,  $k$  is the Boltzmann constant,  $T$  is the junction  
 157 temperature in kelvin and  $q$  is equal to the charge of an electron.

158 In this paper, the first method was used to estimate the thermal voltage due to its simplicity and it does  
 159 not require the estimation of the ideality factor for the PV modules [18]. The estimation of the ideality  
 160 factor is usually cannot be calculated using the maximum power point tracking units provided in the PV  
 161 systems. However, the first method does contain all parameters which are normally available to the user  
 162 of the grid-connected PV (GCPV) plants.

163 The estimation of  $V_{te}$  for the PV module used in this paper under various irradiance levels (100~1000  
 164  $W/m^2$ ) are shown in Fig. 4. The PV module temperature for all measurements is at STC 25 °C and the  
 165 solar cell parameters used in the simulation are shown in Table1.

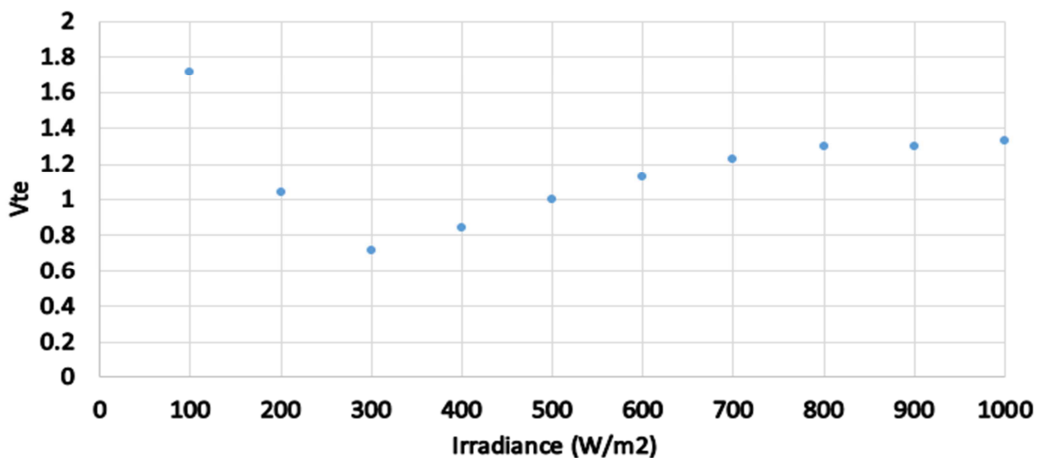


Fig. 4. Thermal Voltage Estimation under Various Irradiance Levels

### 166 3.2 Fill factor (FF)

167 The fill factor (FF) is a generic diagnostic indicator which is sensitive to power losses due to shading and  
 168 faulty conditions occurring in PV systems [27]. FF is sufficiently robust to the irradiance change and the  
 169 temperature levels. FF can be calculated using (5).

$$170 \quad FF = \frac{I_{mp} V_{mp}}{I_{sc} V_{oc}} \quad (5)$$

171 The fill factor is a good indicator since it depends on the voltage and current changes in the PV modules.  
 172 Fig. 5(a) shows the I-V curve of the PV module used in this work. Also it shows the location of the  
 173 parameters used in the calculation of the FF indicator.

174 At STC, the PV module used in this work can be evaluated as shown in (6).

$$175 \quad FF = \frac{I_{mp} V_{mp}}{I_{sc} V_{oc}} = \frac{7.67 \times 28.7}{8.18 \times 36.74} = 73.25\% \quad (6)$$

176 Fig. 5(b) shows the variations of the FF under various irradiance levels (100~1000 W/m<sup>2</sup>).

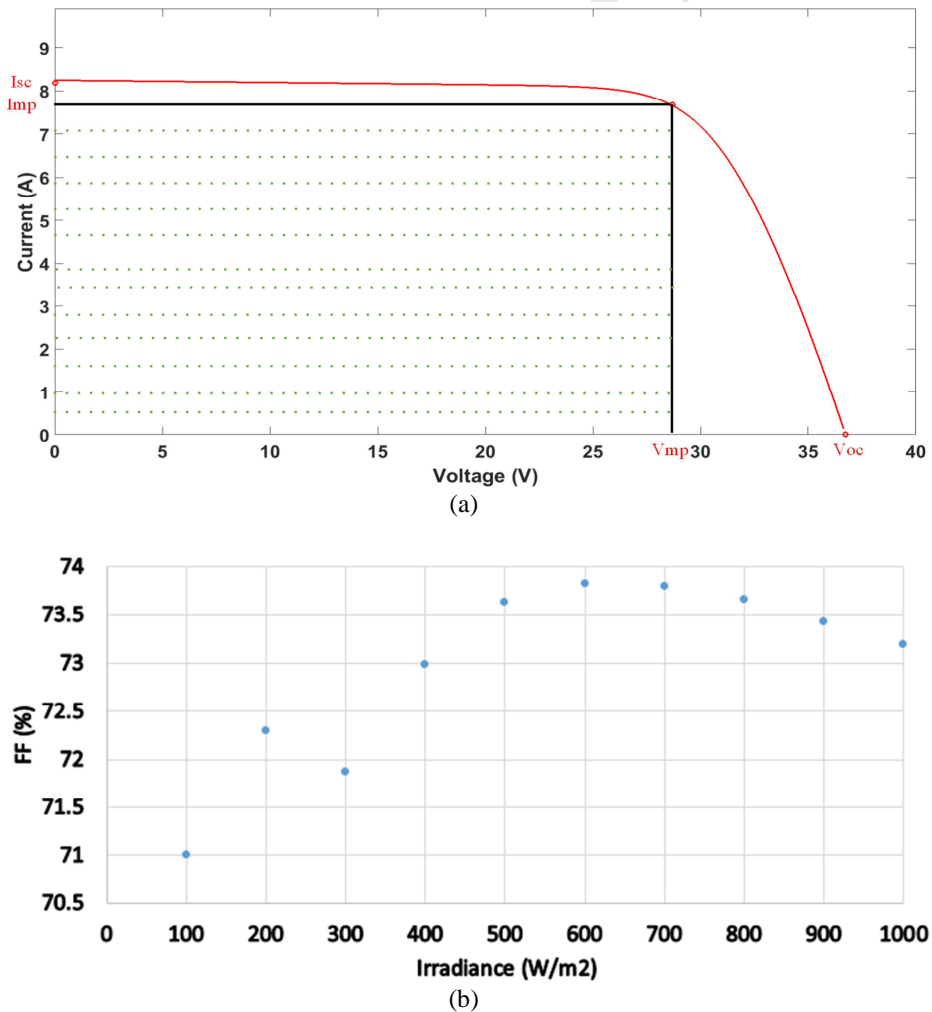


Fig. 5. (a) Fill Factor Parameters Estimation Using Photovoltaic I-V Curve, (b) Fill Factor Estimation under Various Irradiance Levels

177 **3.3 PV series resistance ( $R_s$ )**

178 **Method 1:**

179 One commonly used method to estimate  $R_s$  is to evaluate the derivative of the voltage with respect to the  
180 current at the  $V_{oc}$ . The final expression to approximate the series resistance is described by (7).

181 
$$R_{s,e} = - \frac{dV}{dI} \Big|_V \approx V_{oc} = - \frac{V_2 - V_1}{I_2 - I_1} \Big|_V \approx V_{oc} \quad (7)$$

182 where  $V_2$ ,  $V_1$ ,  $I_2$  and  $I_1$  are the voltage and the current points estimated near to  $V_{oc}$ .

183 The value of the series resistance estimated by the derivative may vary with the irradiance the temperature  
184 conditions [28]. D. Sara et al [29] proposed a method to translate the value of the estimated  $R_s$  to STC in  
185 order to mitigate the effect of the irradiance ( $G$ ) and PV module temperature ( $T$ ). The expression is  
186 illustrated by (8).

187 
$$R_s = R_{s,e} + \frac{V_{te}}{I_{sc}} \left( \frac{G}{G_{STC}} \times \frac{T_{STC}}{T} - 1 \right)$$
  
188 (8)

189 where  $G_{STC}$  is equal to  $1000 \text{ W/m}^2$  and  $T_{STC}$  is equal to  $25 \text{ }^\circ\text{C}$ .

190 As can be noticed, the estimation of the series resistance requires the voltage and the current  
191 measurements of at least two point of the I-V curve close to the  $V_{oc}$ . The method also requires the value  
192 of the irradiance and the PV modules temperature to perform the estimation of the series resistance value.

193 **Method 2:**

194 Another method of estimating the series resistance of a PV module is to evaluate the derivative of the  
195 voltage with respect to the current at the short circuit and maximum power point, such point is  
196 characterized by a current lower, but closer to  $I_{mpp}$  and it is denominated as Q. This method was proposed  
197 by [21] and used in [27 and 28] for the estimation of  $R_s$ . There are two options to calculate Q (9 & 10).

198 
$$Q1 = I_{sc,e} - (0.75 \times I_{mpp}) \quad (9)$$

199 
$$Q2 = I_{sc,e} - (0.60 \times I_{mpp}) \quad (10)$$

200 where the value of  $I_{sc,e}$  is the estimated short circuit current and can be evaluated using (11).

201 
$$I_{sc,e} = \frac{I_{sc}}{K_1} \quad (11)$$

202 where  $K_1$  is the ratio between  $I_{mpp}$  and  $I_{sc}$  and it is assumed as constant value of 0.92 as described by [21].

203 The final expression of estimating the value of the series resistance is expressed by (12).

204 
$$R_s = - \frac{dV}{dI} \Big|_I \approx Q = - \frac{V_2 - V_1}{I_2 - I_1} \Big|_I \approx Q \quad (12)$$

205 The evaluation of the series resistance requires at least two points of the I-V curve for the PV module.  
206 Furthermore, it is required to measure:

- 207 1. Current at maximum power point ( $I_{mpp}$ )  
208 2. Short circuit current ( $I_{sc}$ )

209 Fig. 6 shows the value of the series resistance estimated using method 1 and method 2. The estimated  
 210 values of the  $R_s$  are compared with the measured  $R_s$ . Therefore, the difference between the measured  
 211 values with the estimated values can be expressed by (13).

$$212 \quad \text{Difference} = \text{Estimated } R_s - \text{Measured } R_s \quad (13)$$

213 Table 2 shows the comparison between the estimated  $R_s$  and measured  $R_s$  using method 1: at  $V_{oc}$ , and  
 214 method 2: at Q1 and Q2. The minimum average difference is equal to 1.71% obtained for method 1.  
 215 Therefore, in this paper, method 1 is used for the estimation of  $R_s$ .

Table 2  
 Difference between Estimated  $R_s$  and Measured  $R_s$

Irradiance level ( $W/m^2$ )	Measured $R_s$ ( $\Omega$ )	Estimated $R_s$ ( $\Omega$ ) using method 1		Estimated $R_s$ ( $\Omega$ ) using method 2, Q1		Estimated $R_s$ ( $\Omega$ ) using method 2, Q2	
		$R_s$ ( $\Omega$ )	Difference	$R_s$ ( $\Omega$ )	Difference	$R_s$ ( $\Omega$ )	Difference
1000	0.48484	0.512558	0.027717	0.532558	0.047718	0.582558	0.097718
900	0.537836	0.545554	0.007718	0.595554	0.057718	0.595554	0.057718
800	0.567762	0.58548	0.017718	0.62548	0.057718	0.70548	0.137718
700	0.623004	0.637755	0.014751	0.681755	0.058751	0.687755	0.064751
600	0.698996	0.706714	0.007718	0.606714	-0.09228	0.816714	0.117718
500	0.789787	0.804505	0.014718	0.837845	0.048058	0.934505	0.144718
400	0.934482	0.9522	0.017718	0.9822	0.047718	1.1322	0.197718
300	1.172762	1.20048	0.027718	1.23448	0.061718	1.31048	0.137718
200	1.688184	1.705902	0.017718	1.729902	0.041718	1.815902	0.127718
100	3.240672	3.25839	0.017718	3.28139	0.040718	3.33839	0.097718
		Average Difference (%)		Average Difference (%)		Average Difference (%)	
		1.71		3.69		11.81	

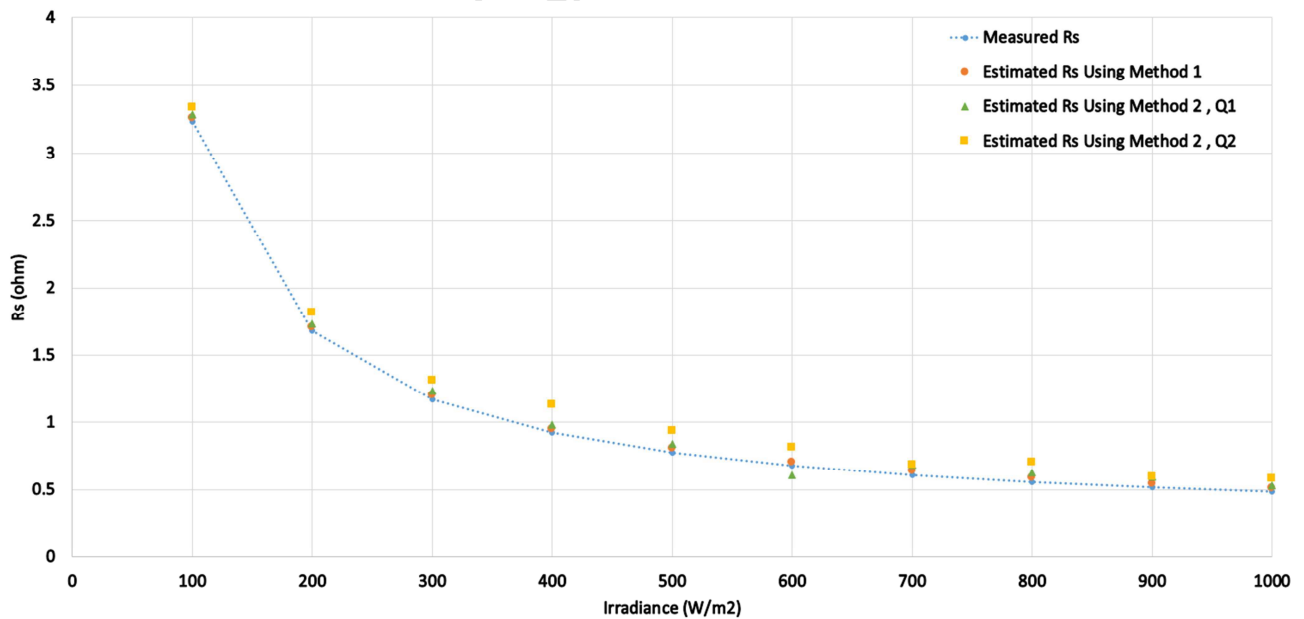


Fig. 6. Evaluating the Series Resistance of a PV Module under Various Irradiance Levels

#### 216 4. Simulation, modelling and data analysis of multiple PV array configurations

217 The aim of this section is to present the multiple PV array configurations used in this study. In order to  
 218 test the multiple PV array configurations, 24 PV modules were used. Each PV module consists of 60 PV  
 219 modules connected in series and protected by bypass diodes. The PV modules temperature was fixed at  
 220 the standard test condition (STC) 25 °C.

##### 221 4.1 Types of examined PV array configurations

222 Five common PV array configurations were used in order to examine the main indicators which are  
 223 mostly changeable during the normal operation mode, partial shading and faulty PV conditions. The  
 224 examined PV array configurations are listed as the following:

- 225 1. Series (S) configuration
- 226 2. Parallel (P) configuration
- 227 3. Series-Parallel (SP) configuration
- 228 4. Total-Cross-Tied (TCT) configuration
- 229 5. Bridge-Linked (BL) configuration

230 MATLAB/Simulink software is used to create the listed PV array configurations. Appendix A contains all  
 231 MATLAB/Simulink software models which are used to configure the grid-connected PV (GCPV)  
 232 systems. Furthermore, during the simulation all indicators:  $V_{mpp}$ ,  $V_{oc}$ ,  $I_{mpp}$ ,  $I_{sc}$ ,  $P_{mpp}$ ,  $R_s$ , FF and  $V_{te}$  were  
 233 saved in a spreadsheet to evaluate the performance of each PV array configuration separately.

##### 234 4.2 PV array configurations under STC

235 This section presents the variations of all required indicators at standard test conditions applied to the PV  
 236 array configurations. Table 3 shows the value of all indicators for the different PV array configurations.  
 237 The main outcomes from the obtained results can be expressed by the following:

- 238 1. Series configuration: the dominant indicator is the value of the  $V_{oc}$ ,  $V_{mp}$  and the value of the  
 239 thermal voltage.
- 240 2. Parallel configuration:  $I_{sc}$ ,  $I_{mpp}$  and the thermal voltage which has the least value across all PV  
 241 configurations.
- 242 3. SP, TCT and BL configurations have a common similarity across all indicators.
- 243 4. At STC, the FF for all PV configurations is approximately equal to 73.2%.

244 From Table 4 it is possible to evaluate the value of the series resistance across one PV module in the

Table 3  
 Mathematical Calculations of  $R_s$  for Various GCPV Plants

PV array configuration	Mathematical expression for estimating the value of $R_s$ for one PV module in the PV array configuration	
S	$\frac{R_s \text{ (Obtained from the } I-V \text{ Curve)}}{24_{\text{(total PV module in the PV array configuration)}}$	(14)
P	$R_s \text{ (Obtained from the } I-V \text{ Curve)} \times 24_{\text{(total PV module in the PV array configuration)}}$	(15)
SP, TCT and BL	$\frac{R_s \text{ (Obtained from the } I-V \text{ Curve)} \times 4_{\text{(number of PV columns)}}}{6_{\text{(number of PV modules in one PV row "PV String")}}}$	(16)

245 GCPV systems according to the mathematical expressions listed below in Table 3.

246 Table 5 shows that the estimation of the series resistance for a single PV module using the mathematical  
 247 expressions listed in Table 3 at STC. There is a slightly difference between the real measured  $R_s$  values at  
 248 STC with the calculated  $R_s$  using (14-16). The percentage of the average difference between the measured

Table 4  
 Indicators Values Estimated for All Examined PV Array Configurations

PV configuration	$I_{sc}$ (A)	$V_{oc}$ (V)	$I_{mpp}$ (A)	$V_{mpp}$ (V)	$P_{mpp}$ (W)	$R_s$ ( $\Omega$ )	$V_{te}$ (V)	FF (%)
S	8.177	881.2	7.538	700.3	5279	12.18175	36.2059	73.2608
P	196.2	36.74	181.4	29.1	5279	0.020116	1.44597	73.2305
SP	32.71	220.3	30.26	174.4	5279	0.757576	8.59957	73.2353
TCT	32.71	220.3	30.33	174	5278	0.757576	8.31149	73.2363
BL	32.71	220.3	30.33	174	5278	0.757576	8.31149	73.2363

Table 5  
 Estimated  $R_s$  for One PV Module Only

PV configuration	$R_s$ ( $\Omega$ )	Calculated $R_s$ for one PV module ( $\Omega$ )	Measured $R_s$ for one PV module at STC ( $\Omega$ )	Difference in the estimation of $R_s$ (%)
S	12.18175	0.507573	0.48484	2.273299
P	0.020116	0.482772	0.48484	-0.20675
SP	0.757576	0.505051	0.48484	2.021051
TCT	0.757576	0.505051	0.48484	2.021051
BL	0.757576	0.505051	0.48484	2.021051

249  $R_s$  and the calculated  $R_s$  is equal to 2.2%.

### 250 4.3 Partial shading conditions applied to the PV array configurations

251 In order to evaluate the behavior of each PV configuration under non-uniform irradiance conditions and  
 252 to choose the most optimal configuration that provides that highest performance and identifying the main  
 253 indicators which are changing significantly in each PV configuration, two different shading scenarios and  
 254 two faulty PV conditions were tested for each PV configuration under a fixed temperature 25 °C.

#### 255 4.3.1 Scenario 1: row level

256 In this part, the focus will be on the performance of the PV configurations which are affected by a  
 257 uniformly and non-uniform shading patterns on a row level (row of PV modules). Fig. 7 shows both  
 258 patterns used to evaluate the row shading conditions effects on the PV modules.

259 As can be noticed from Fig. 7, two different partial shading conditions was performed. The first partial  
 260 shading pattern is applied on a row of PV modules at irradiance level equal to 500 W/m<sup>2</sup>. However, the  
 261 second shading pattern consists of various irradiance levels (200, 400, 600 and 800 W/m<sup>2</sup>) applied to four  
 262 PV modules.

263 Fig. 8(a) shows the maximum output power obtained in each PV array configuration under shading  
 264 pattern 1. The P configuration shows the maximum output power comparing to all other examined PV  
 265 array configurations. The configurations S, SP, TCT and BL provide the same maximum power in each  
 266 case.

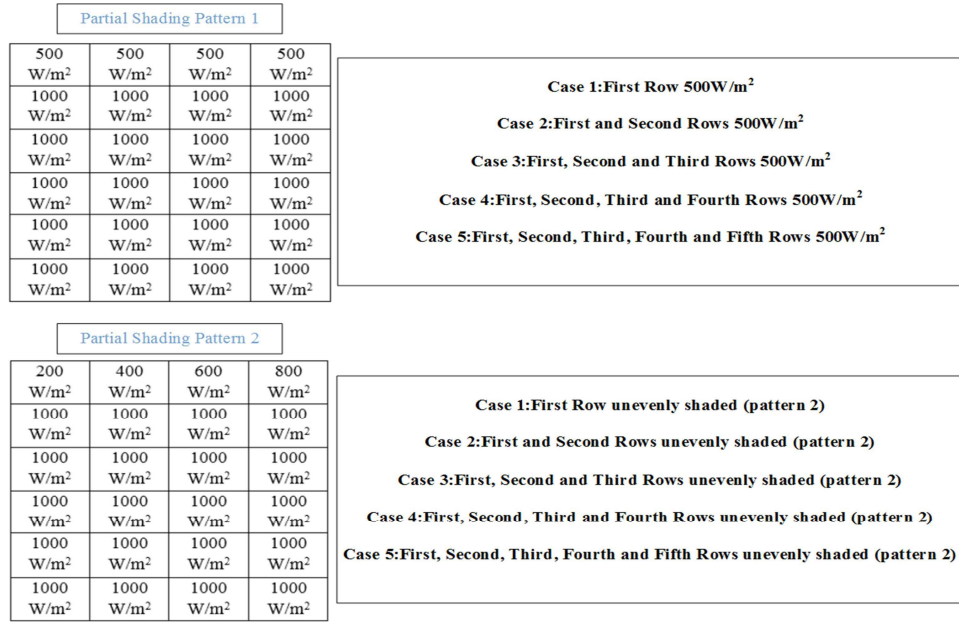


Fig. 7. Partial Shading Patterns for Scenario 1: Row Level

267 Fig. 8(b) proves that P configuration has the maximum output power among all other PV array  
 268 configurations under shading pattern 2. TCT and BL comes second best choice whereas the series  
 269 configuration has the lowest performance.

270 In each shading pattern, the series resistance ( $R_s$ ) was estimated using method 1 which has been discussed  
 271 previously in section 3.3. Table 6 shows the estimated  $R_s$  for each PV array configuration for shading  
 272 pattern 1.  $R_s$  estimated for the S configuration is increased by approximate to 1.13  $\Omega$ . Additionally, the  
 273 estimated series resistance for SP, TCT and BL configurations is increased by approximate to 0.07  $\Omega$ .  
 274 There is a very small amount of change in the series resistance obtained for P configuration, the reduction  
 275 is only equal to 0.002  $\Omega$ .

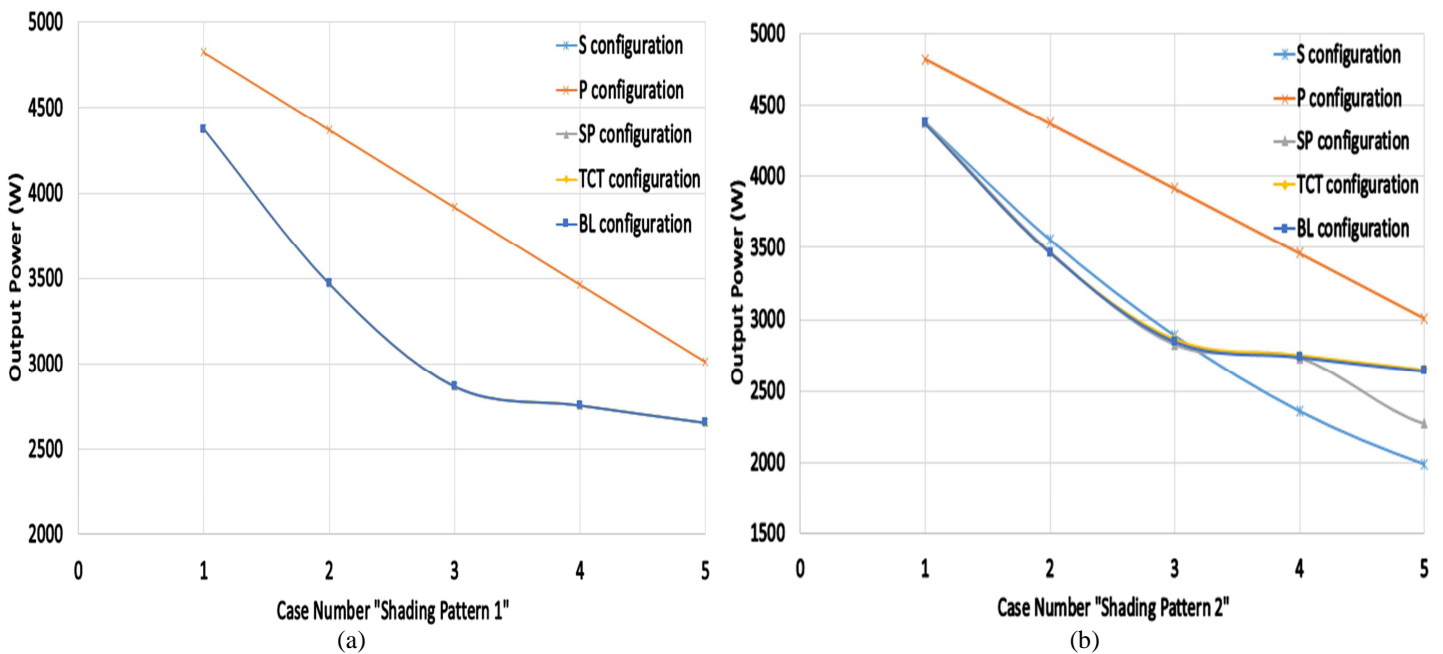


Fig. 8. Partial Shading Patterns for Scenario 1: Row Level. (a) Output Power for Pattern 1, (b) Output power for Pattern 2

Table 6

Estimated  $R_s$  for the Multiple Array Configurations, Scenario 1: Row Level, Pattern 1

Case #	Estimated $R_s$ ( $\Omega$ ) for Shading Pattern 1				
	S	P	SP	TCT	BL
Case 1	13.33689	0.022147	0.826446	0.826446	0.826446
Case 2	14.47387	0.023601	0.897666	0.897666	0.897666
Case 3	15.61524	0.025198	0.966184	0.966184	0.966184
Case 4	16.7392	0.027174	1.037344	1.037344	1.037344
Case 5	17.87949	0.029661	1.105705	1.105705	1.105705

Table 7

Estimated  $R_s$  for the Multiple Array Configurations, Scenario 1: Row Level, Pattern 2

Case #	Estimated $R_s$ ( $\Omega$ ) for Shading Pattern 2				
	S	P	SP	TCT	BL
Case 1	14.05877	0.022279	0.848896	0.827267	0.835422
Case 2	15.9261	0.023609	0.921404	0.898473	0.906618
Case 3	17.75884	0.025253	0.990099	0.968992	0.975039
Case 4	19.604	0.027216	1.053297	1.037775	1.045369
Case 5	21.42704	0.029775	1.136493	1.109385	1.117318

276 Table 7 shows the estimated  $R_s$  for partial shading pattern 2. The S configuration has an increase by 1.8  $\Omega$   
 277 in the  $R_s$ . Moreover, the parallel configuration has the lowest rate of change in the  $R_s$  which is  
 278 approximate equal to 0.002. SP, TCT and BL configurations has an increase of 0.07  $\Omega$  in the  $R_s$  among all  
 279 testes cases in the row level partial shading conditions.

280 The FF indicator was also calculated for each examined partial shading patterns. Fig. 9(a) and Fig 9(b)  
 281 illustrates the FF variations among the tested GCPV systems for shading pattern 1 and shading pattern 2  
 282 respectively. The P configuration shows that the FF has a value close to 73% among all tested case  
 283 scenarios. However, a reduction in the FF was obtained across all other PV array configurations.

284 The Thermal voltage  $V_{te}$  across each PV array configuration during the tested partial shading pattern1 and  
 285 pattern 2 are shown in Fig. 9(c) and Fig. 9(d) respectively. The threshold values of the  $V_{te}$  is taken from  
 286 Table 4. It is evident that the  $V_{te}$  for P configuration is approximate equal to 1.44V which is exactly the  
 287 same as the P configuration  $V_{te}$  threshold.

288 S, SP, TCT and BL configurations show that the value of  $V_{te}$  is lower than the value of  $V_{te}$  threshold in  
 289 low partial shading conditions if: reduction in irradiance  $< 6000 \text{ W/m}^2$ . However, in most partial shading  
 290 conditions examined in this section, the obtained value of the  $V_{te}$  is greater than the value of  $V_{te}$  threshold  
 291 if: reduction in the irradiance  $\geq 6000 \text{ W/m}^2$ .

292 From this section, the obtained results could be illustrated as the following:

- 293
- 294 •  $R_s$  could be a good indicator to predict/estimate partial shading conditions for S, SP, TCT and BL  
 295 configurations. However,  $R_s$  cannot be used with P configuration since it does not change  
 296 significantly during the increase/decrease of the partial shading conditions applied PV system.
  - 297 • FF has a significant drop in its value while increasing the partial shading in the S, SP, TCT and  
 298 BL configurations. This is not a proper indicator to be used with P configuration since it does not  
 299 change among all tested partial shading conditions.
  - 300 • When the reduction in the irradiance is greater or equal to  $6000 \text{ W/m}^2$ , the value of the  $V_{te}$  in most  
 301 partial shading conditions is greater than the value of  $V_{te}$  threshold for S, SP, TCT and BL  
 302 configurations. However, P configurations shows that the value of the  $V_{te}$  is almost equal to the  
 value of  $V_{te}$  threshold.

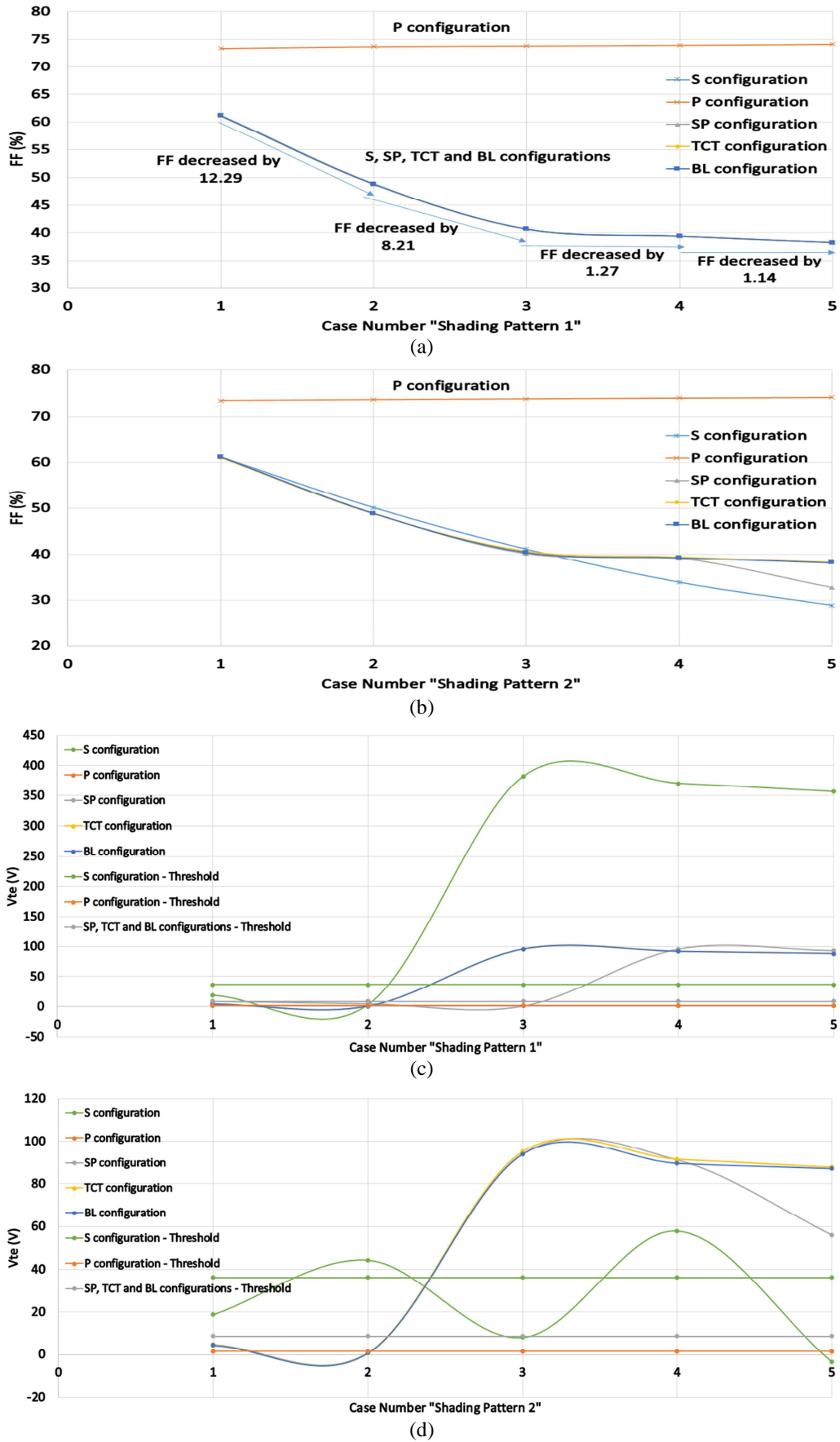


Fig. 9. FF and  $V_{te}$  Variations for Scenario 1: Row Level. (a) Fill Factor Variations for Pattern 1, (b) Fill Factor Variations for Pattern 2, (c)  $V_{te}$  Variations for Pattern 1, (d)  $V_{te}$  Variations for Pattern 2

### 303 4.3.2 Scenario 2: column level

304 This section is created to check the variations of the  $R_s$ ,  $V_{te}$ , FF indicators when a partial shading  
305 conditions occurred in the PV array configuration on a column level (column of PV modules).

306 Fig. 10 shows two different partial shading patterns examined. The first partial shading pattern is applied  
307 on a column of PV modules at irradiance level equal to  $500 \text{ W/m}^2$ . However, the second shading pattern  
308 consists of various irradiance levels (100, 200, 500, 600, 800 and  $900 \text{ W/m}^2$ ) applied to six PV modules.

309 Fig. 11(a) shows the maximum output power obtained in each PV array configuration under shading  
310 pattern 1. P, SP, TCT and BL configurations shows approximately the same maximum output power.  
311 Furthermore, S configuration provides the minimum output power during all examined case scenarios  
312 used in shading pattern 1. On the other hand, the maximum output power obtained from shading pattern 2  
313 is illustrated in Fig. 11(b). The maximum output power could be evaluated at the P configuration.  
314 However, S configuration remains the worst configuration.

315 In each shading pattern (pattern 1 and 2), the series resistance ( $R_s$ ) was estimated. Table 8 shows the  
316 estimated  $R_s$  for each PV array configuration for shading pattern 1. As can be noticed,  $R_s$  estimated for  
317 the S configuration is increasing by approximate to  $1.68 \Omega$ . This result can be calculated using the  
318 difference between case1 and case2, where the values of  $R_s$  are taken from the measured data explained in  
319 table 2:

$$\text{Estimated } R_s = \text{Number of PV modules (at partial shading condition)} \times R_s \text{ (at partial shading condition)}$$

$$\text{Case1: Estimated } R_s = \left( 6_{\left( \text{at } 500 \frac{\text{W}}{\text{m}^2} \right)} \times 0.789787 \right) + \left( 18_{\left( \text{at } 1000 \frac{\text{W}}{\text{m}^2} \right)} \times 0.48484 \right) = 13.47 \Omega$$

$$\text{Case2: Estimated } R_s = \left( 12_{\left( \text{at } 500 \frac{\text{W}}{\text{m}^2} \right)} \times 0.789787 \right) + \left( 12_{\left( \text{at } 1000 \frac{\text{W}}{\text{m}^2} \right)} \times 0.48484 \right) = 15.30 \Omega$$

320  $\text{Difference} = \text{Case2} - \text{Case1} = 15.3 - 13.47 = 1.83 \Omega \approx 1.68 \Omega$  Obtained by the I – V cuve

Partial Shading Pattern 1			
500 W/m <sup>2</sup>	1000 W/m <sup>2</sup>	1000 W/m <sup>2</sup>	1000 W/m <sup>2</sup>
500 W/m <sup>2</sup>	1000 W/m <sup>2</sup>	1000 W/m <sup>2</sup>	1000 W/m <sup>2</sup>
500 W/m <sup>2</sup>	1000 W/m <sup>2</sup>	1000 W/m <sup>2</sup>	1000 W/m <sup>2</sup>
500 W/m <sup>2</sup>	1000 W/m <sup>2</sup>	1000 W/m <sup>2</sup>	1000 W/m <sup>2</sup>
500 W/m <sup>2</sup>	1000 W/m <sup>2</sup>	1000 W/m <sup>2</sup>	1000 W/m <sup>2</sup>
500 W/m <sup>2</sup>	1000 W/m <sup>2</sup>	1000 W/m <sup>2</sup>	1000 W/m <sup>2</sup>

Case 1: First Column  $500 \text{ W/m}^2$

Case 2: First and Second Columns  $500 \text{ W/m}^2$

Case 3: First, Second and Third Columns  $500 \text{ W/m}^2$

Case 4: First, Second, Third and Fourth Columns  $500 \text{ W/m}^2$

Partial Shading Pattern 2			
100 W/m <sup>2</sup>	1000 W/m <sup>2</sup>	1000 W/m <sup>2</sup>	1000 W/m <sup>2</sup>
200 W/m <sup>2</sup>	1000 W/m <sup>2</sup>	1000 W/m <sup>2</sup>	1000 W/m <sup>2</sup>
500 W/m <sup>2</sup>	1000 W/m <sup>2</sup>	1000 W/m <sup>2</sup>	1000 W/m <sup>2</sup>
600 W/m <sup>2</sup>	1000 W/m <sup>2</sup>	1000 W/m <sup>2</sup>	1000 W/m <sup>2</sup>
800 W/m <sup>2</sup>	1000 W/m <sup>2</sup>	1000 W/m <sup>2</sup>	1000 W/m <sup>2</sup>
900 W/m <sup>2</sup>	1000 W/m <sup>2</sup>	1000 W/m <sup>2</sup>	1000 W/m <sup>2</sup>

Case 1: First Column unevenly shaded (pattern 2)

Case 2: First and Second Columns unevenly shaded (pattern 2)

Case 3: First, Second and Third Columns unevenly shaded (pattern 2)

Case 4: First, Second, Third and Fourth Columns unevenly shaded (pattern 2)

Fig. 10. Partial Shading Patterns for Scenario 2: Column Level

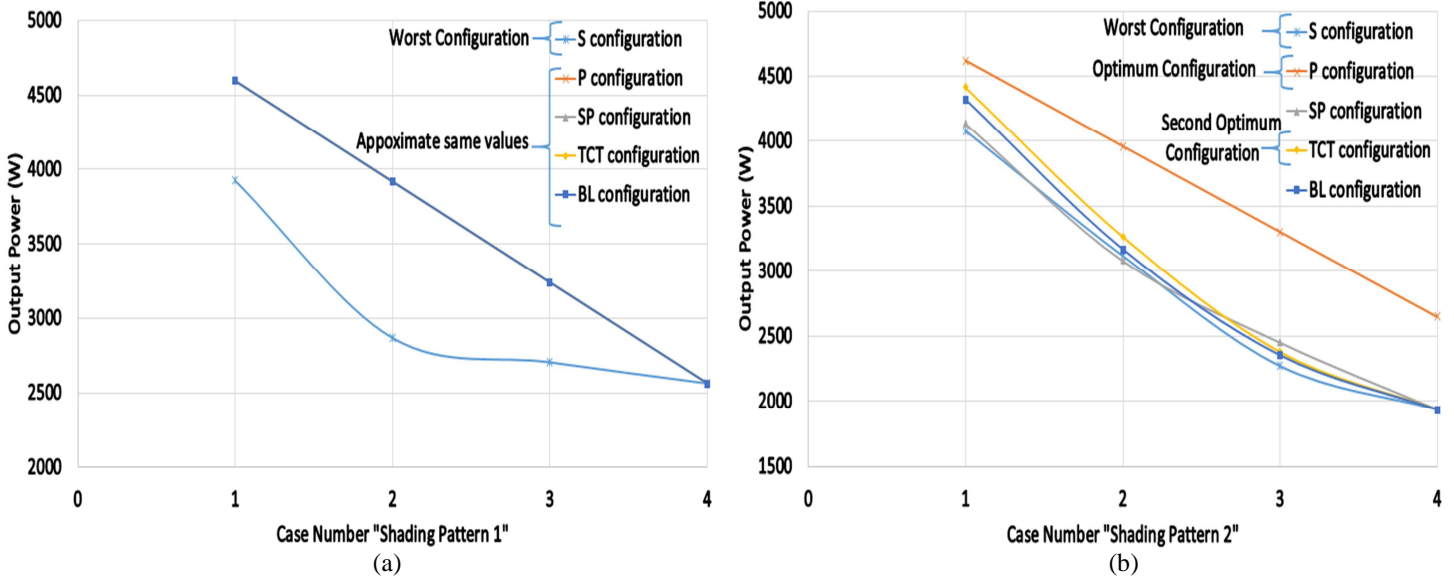


Fig. 11. Partial Shading Patterns for Scenario 2: Column Level. (a) Output Power for Pattern 1, (b) Output power for Pattern 2

321 Additionally, the estimated series resistance for SP, TCT and BL configurations is increasing by  
 322 approximate to  $0.12 \Omega$ . However, the parallel configuration remains at nearly constant series resistance  
 323 between  $0.02 - 0.03 \Omega$ .

324 For the second shading pattern (non-uniform irradiance) the estimated  $R_s$  for SP, TCT and BL  
 325 configurations is increasing by  $0.3 \Omega$ . The parallel configuration remains at the same  $R_s$  which is between  
 326  $0.02 - 0.03 \Omega$ . Similarly, the estimated series resistance for S configuration is increasing by  $4.4 \Omega$  while  
 327 increasing the applied partial shading on the PV array configuration, this can be seen in Table 9 and  
 328 described by the following mathematical calculations, where the values of  $R_s$  are taken from the measured  
 329 data explained in table 2:

$$\text{Measured } R_s = \text{Number of PV modules (at partial shading condition)} \times R_s \text{ (at partial shading condition)}$$

Case1: Measured  $R_s$

$$\begin{aligned} &= \left( 1_{\left( \text{at } 100 \frac{W}{m^2} \right)} \times 3.241 \right) + \left( 1_{\left( \text{at } 200 \frac{W}{m^2} \right)} \times 1.688 \right) + \left( 1_{\left( \text{at } 500 \frac{W}{m^2} \right)} \times 0.789787 \right) \\ &+ \left( 1_{\left( \text{at } 600 \frac{W}{m^2} \right)} \times 0.6988 \right) + \left( 1_{\left( \text{at } 800 \frac{W}{m^2} \right)} \times 0.5677 \right) + \left( 1_{\left( \text{at } 900 \frac{W}{m^2} \right)} \times 0.5378 \right) \\ &+ \left( 18_{\left( \text{at } 1000 \frac{W}{m^2} \right)} \times 0.48484 \right) = 16.25 \Omega \end{aligned}$$

Case2: Measured  $R_s$

$$\begin{aligned} &= \left( 2_{\left( \text{at } 100 \frac{W}{m^2} \right)} \times 3.241 \right) + \left( 2_{\left( \text{at } 200 \frac{W}{m^2} \right)} \times 1.688 \right) + \left( 2_{\left( \text{at } 500 \frac{W}{m^2} \right)} \times 0.789787 \right) \\ &+ \left( 2_{\left( \text{at } 600 \frac{W}{m^2} \right)} \times 0.6988 \right) + \left( 2_{\left( \text{at } 800 \frac{W}{m^2} \right)} \times 0.5677 \right) + \left( 2_{\left( \text{at } 900 \frac{W}{m^2} \right)} \times 0.5378 \right) \\ &+ \left( 12_{\left( \text{at } 1000 \frac{W}{m^2} \right)} \times 0.48484 \right) = 20.865 \Omega \end{aligned}$$

Table 8

Estimated  $R_s$  for the Multiple Array Configurations, Scenario 2: Column Level, Pattern 1

Case #	Estimated $R_s$ ( $\Omega$ ) for Shading Pattern 1				
	S	P	SP	TCT	BL
Case 1	13.8754	0.022921	0.818197	0.818197	0.818197
Case 2	15.55936	0.025198	0.898957	0.898957	0.898957
Case 3	17.26519	0.028329	1.012146	1.012146	1.012146
Case 4	18.93581	0.033034	1.176471	1.176471	1.176471

Table 9  
Estimated  $R_s$  for the Multiple Array Configurations, Scenario 2: Column Level, Pattern 2

Case #	Estimated $R_s$ ( $\Omega$ ) for Shading Pattern 2				
	S	P	SP	TCT	BL
Case 1	16.85772	0.022861	0.83675	0.819403	0.823045
Case 2	21.33106	0.025054	0.961538	0.918274	0.929195
Case 3	25.75992	0.02809	1.186662	1.106195	1.119821
Case 4	30.08424	0.032468	1.845018	1.845359	1.845359

330  $Difference = Case2 - Case1 = 20.865 - 16.25 = 4.6 \Omega \approx 4.4 \Omega$  Obtained by the I – V cuve

331 Fig. 12(a) and Fig. 12(b) illustrates the FF variations among the tested PV array configuration systems for  
 332 shading pattern 1 and shading pattern 2 respectively. Shading pattern 1 shows that P, SP, TCT and BL  
 333 configurations have a value of FF approximate to 74% among all tested cases. However, a reduction in  
 334 the FF was only obtained across the S configuration. Shading pattern 2 (non-uniform shading) shows a  
 335 different results comparing to shading pattern 1 (uniform shading), these results could be illustrated as the  
 336 following:

- 337 • The estimated FF for the P configuration under non-uniform and uniform shading patterns are  
 338 exactly equal.
- 339 • There is a huge reduction in the FF for S, SP, TCT and BL configurations in the non-uniform  
 340 shading pattern conditions.
- 341 • Fig. 12(a) shows that the value of the FF for the S configuration at case 4 is equal to 74% because  
 342 in this particular shading case, the percentage of shading among all PV modules are equal.

343 The Thermal voltage  $V_{te}$  across each PV array configuration during the tested partial shading pattern1 and  
 344 pattern 2 are shown in Fig. 12(c) and Fig. 9(d) respectively. The threshold values of the  $V_{te}$  is taken from  
 345 Table 4. It is evident that the  $V_{te}$  for P configuration is approximate equal to 1.44V which is exactly the  
 346 same as the P configuration  $V_{te}$  threshold. The estimated values of the  $V_{te}$  for SP, TCT and BL  
 347 configurations are exactly the same as the  $V_{te}$  threshold during shading pattern 1. However, the estimated  
 348  $V_{te}$  for S configuration is greater than the value of the  $V_{te}$  threshold if: Reduction in irradiance  $\geq 6000$   
 349  $W/m^2$ .

350 Fig. 12(d) shows that the estimated  $V_{te}$  is exactly the same as the  $V_{te}$  threshold for shading pattern 2. SP,  
 351 TCT and BL configurations proves that when the reduction in the irradiance is greater than  $2900 W/m^2$   
 352 the estimated value of  $V_{te}$  is always greater than  $V_{te}$  threshold. Moreover, S configuration shows that the  
 353 value of the  $V_{te}$  is greater than  $V_{te}$  threshold if: Reduction in irradiance  $\geq 6000 W/m^2$ .

354 In conclusion, this section shows some results on the performance of the examined PV array  
 355 configurations under uniform and non-uniform partial shading patterns. The main findings could be  
 356 illustrated as the following:

- 357 • Under uniform shading patterns which effects on a column of PV modules, the output power for  
 358 P, SP, TCT and BL configurations are exactly the same. Furthermore, the S configuration shows  
 359 the least output power among all PV array configurations.
- 360 • Under non-uniform shading patterns which effects on a column of PV modules, the optimum  
 361 output power was estimated for the parallel configuration.
- 362 • The series resistance  $R_s$  is a good indicator for detecting/predicting partial shading conditions for  
 363 S, SP, TCT and BL configurations since the value of the  $R_s$  change significantly while increasing  
 364 the partial shading conditions applied to the PV configurations.
- 365 • The Fill factor (FF) indicator could be used with SP, TCT and BL configurations only under non-  
 366 uniform irradiance conditions. Furthermore, there is a large drop in the value of FF for the S  
 367 configuration under uniform and non-uniform irradiance levels.

- 368  
369  
370
- The value of the  $V_{te}$  could be used as a proper indicator for detecting partial shading conditions for S, SP, TCT and BL configuration under non-uniform partial shading conditions affecting the GCPV plants.

ACCEPTED MANUSCRIPT

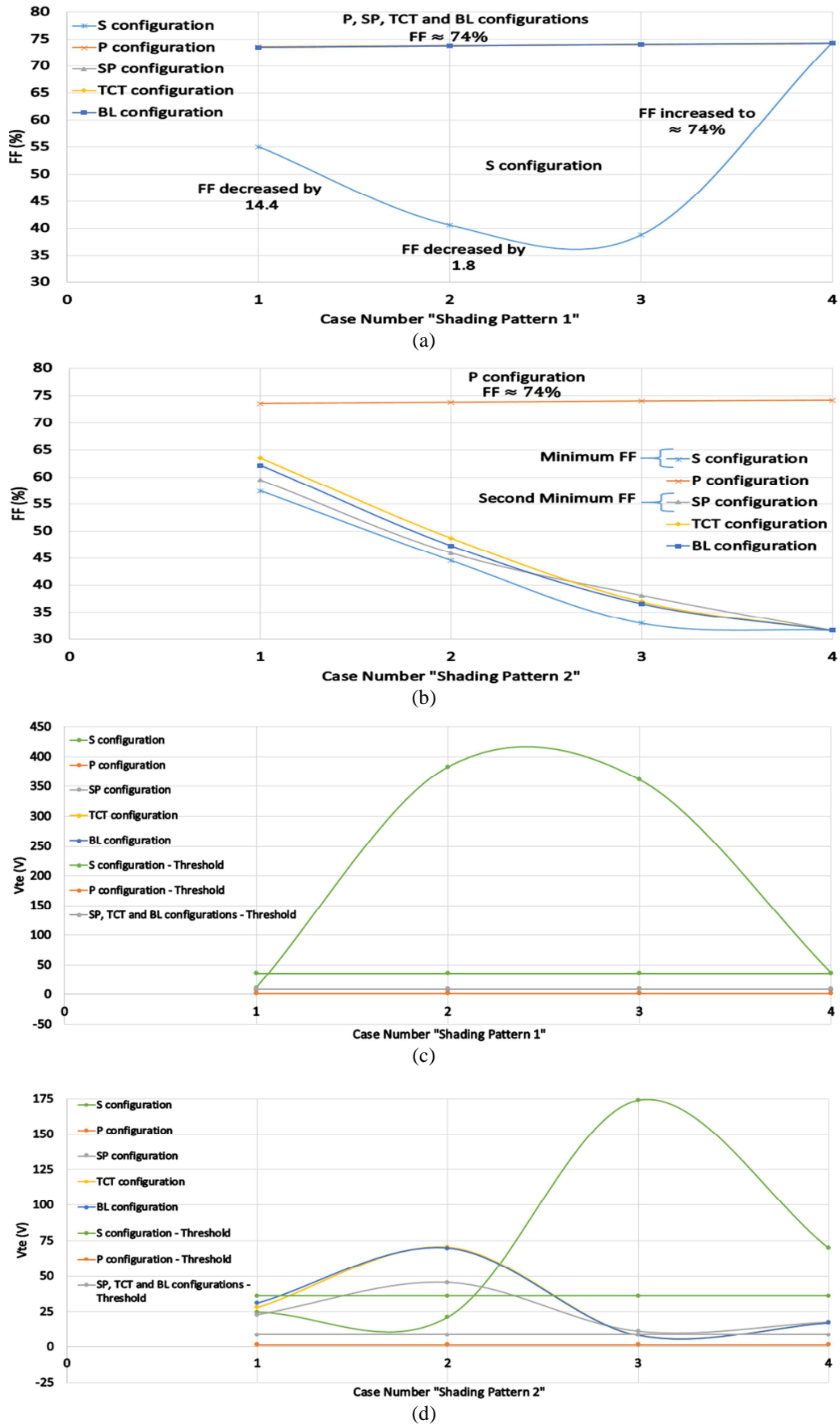


Fig. 12. FF and  $V_{te}$  Variations for Scenario 2: Column Level. (a) Fill Factor Variations for Pattern 1, (b) Fill Factor Variations for Pattern 2, (c)  $V_{te}$  Variations for Pattern 1, (d)  $V_{te}$  Variations for Pattern 2

371 **4.3.3 Scenario 3: faulty PV modules**

372 This section is created to check the variations of the  $R_s$ ,  $V_{te}$ , FF indicators when a faulty PV modules have  
373 been a raised in the PV array configurations.

374 Two faulty scenarios were carried out to estimate the output performance for each PV array configuration  
375 under faulty PV modules. Fig. 13 illustrates both cases which can be described by the following:

- 376 1. Row level: six different scenarios were tested to estimate the faulty PV modules which are  
377 disconnected (short circuit the PV module) from a row of the PV array configuration.
- 378 2. Column level: four different scenarios were tested to estimate the faulty PV modules which are  
379 disconnected from the entire column of the PV array configuration.

380 The PV modules irradiance and temperature level are at standard test conditions:  $1000W/m^2$  and  $25^\circ C$   
381 respectively.

382 Fig. 14(a) and Fig 14(b) shows that the configurations S and P provides the highest maximum output  
383 power among all PV array configurations. The second maximum output power is achieved by the SP  
384 configuration. However, the minimum output power is estimated for the TCT configuration among all  
385 faulty PV case scenarios.

386 The estimated series resistance  $R_s$  for the row-level PV faulty conditions are illustrated in Table 10. The S  
387 configuration shows that  $R_s$  is decreasing by  $0.49 \Omega$  while disconnecting one PV module. This result is  
388 approximate equal to the measured value of  $R_s$  among one PV module ( $0.48484 \Omega$ ) under STC as shown  
389 previously in Table 5.

390 The estimated  $R_s$  for the P configuration among all faulty scenarios is approximately equal to  $0.02 \Omega$ . The  
391 value of  $R_s$  when a PV string is disconnected from the PV array configuration is equal to  $1.007 \Omega$  for SP,  
392 TCT and BL configurations, this value could be calculated using (16) as the following:

$$393 \quad \text{Estimated } R_s \text{ for one PV module} = \frac{R_s \text{ (Obtained from the } I-V \text{ Curve)} \times 3 \text{ (number of PV columns)}}{6 \text{ (number of PV modules in one PV row "PV String")}}$$

$$0.48484 = \frac{R_s \text{ (Obtained from the } I-V \text{ Curve)} \times 3 \text{ (Since one PV string is completely disconnected)}}{6}$$

$$R_s \text{ (Obtained from the } I-V \text{ Curve)} = 0.97 \Omega \approx 1.007 \Omega$$

394 The estimated series resistance  $R_s$  for the column-level PV faulty conditions are illustrated in Table 11.  
395 As can be noticed that the value of  $R_s$  in the S and SP configurations is decreased while increasing the  
396 number of faulty PV modules. The estimated  $R_s$  for TCT and BL is increasing for the first three PV faulty  
397 conditions. However, the estimated  $R_s$  is equal to  $0.63 \Omega$  when disconnecting an entire PV column form  
398 the SP, TCT and BL array configurations. This result could be estimated using (16) as the following:

$$399 \quad \text{Estimated } R_s \text{ for one PV module} = \frac{R_s \text{ (Obtained from the } I-V \text{ Curve)} \times 4 \text{ (number of PV columns)}}{5 \text{ (number of PV modules in one PV row "PV String")}}$$

$$0.48484 = \frac{R_s \text{ (Obtained from the } I-V \text{ Curve)} \times 4 \text{ (Since one PV string is completely disconnected)}}{5}$$

$$R_s \text{ (Obtained from the } I-V \text{ Curve)} = 0.61 \Omega \approx 0.63 \Omega$$

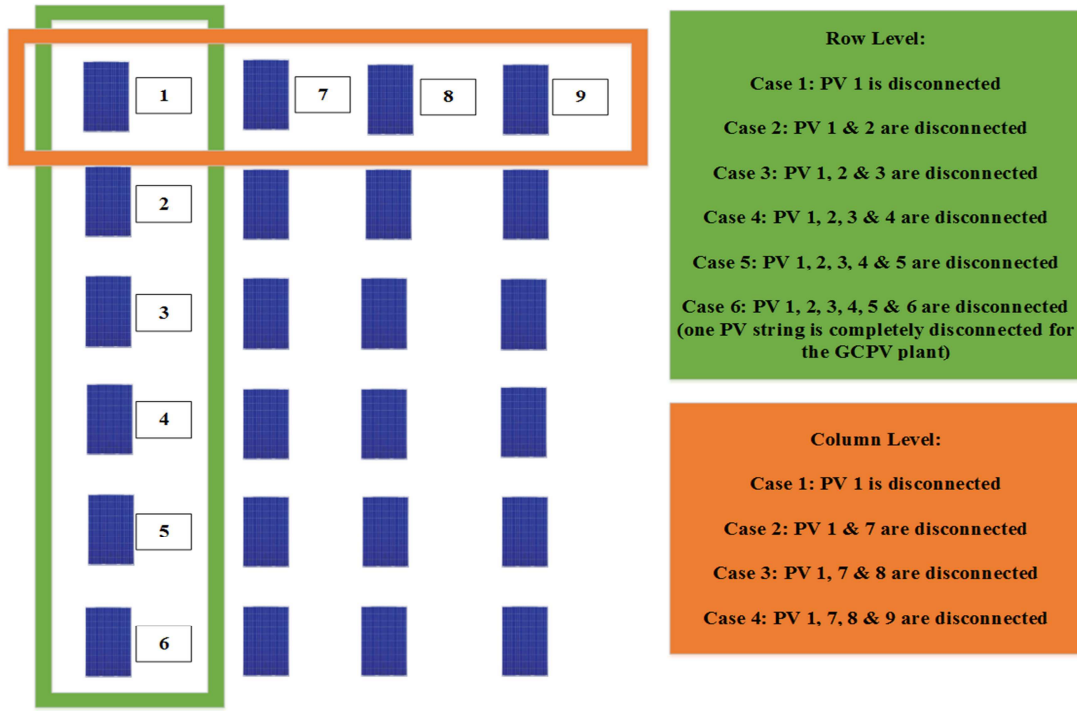


Fig. 13. PV Faulty Conditions for Scenario 3: Faulty PV Modules

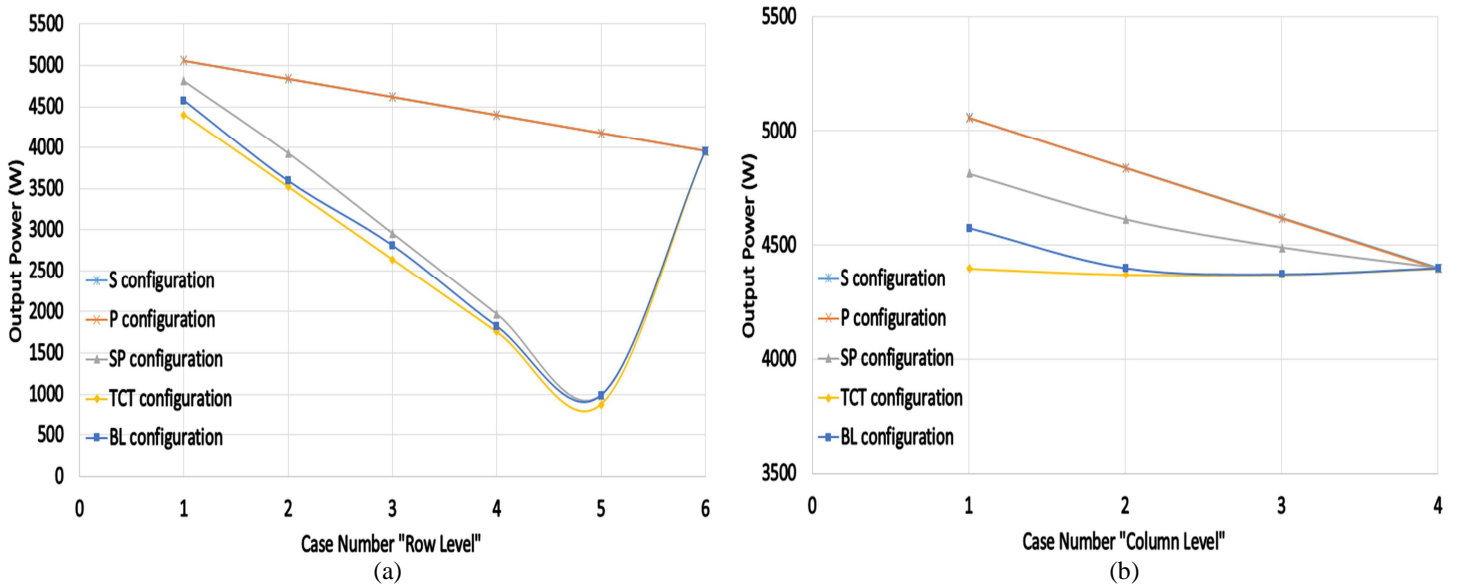


Fig. 14. Output Power for Scenario 3: Faulty PV Modules. (a) Output Power for Pattern 1, (b) Output power for Pattern 2

400 Fig. 15(a) and Fig. 15(b) illustrates the FF variations among the tested PV array configurations using  
 401 faulty conditions: row-level and column level respectively. Row-level PV faulty conditions show that S, P  
 402 and TCT configurations have a value of FF approximate to 73.2% among all tested scenarios. However, a  
 403 reduction in the FF was only obtained across the SP and BL configurations.

404 The column-level PV faulty conditions shows that the FF for the S and P configuration remains at 73.2%.  
 405 Furthermore, there is a huge reduction in the estimated FF for both TCT and BL configurations. The only  
 406 configuration which has an increase in the estimated values of the FF was obtained for the SP  
 407 configuration.

408 As shown in Fig. 15(a) at case 6 (Faulty PV string) the estimated value of the FF across all PV array  
 409 configurations is equal to 73.2%. Similar results obtained for case4 (faulty column) illustrated in Fig  
 410 15(b).

411 The Thermal voltage  $V_{te}$  estimated for each PV array configuration under faulty PV modules conditions  
 412 (row-level and column-level) are shown in Fig. 15(c) and Fig. 9(d) respectively. From Fig. 15(c), it is  
 413 evident that  $V_{te}$  for P configuration is equal to 1.36V among all PV faulty conditions, this result is  
 414 approximately equal to P configuration  $V_{te}$  threshold: 1.44V. The estimated value of the  $V_{te}$  for S, SP,  
 415 TCT and BL configurations is decreased while increasing the number of faulty PV modules in the PV  
 416 array configuration due to the decrease in the  $V_{mp}$ . Despite the decrease of  $V_{oc}$ , the value of  $V_{mp}$  is  
 417 multiplied by a factor of 2, therefore,  $V_{te}$  is also decreasing. This results can be expressed by the  
 418 following:

$$419 \quad V_{te} \downarrow = \frac{(2V_{mp} \downarrow - V_{oc} \downarrow)(I_{sc} - I_{mp})}{I_{mp} - (I_{sc} - I_{mp}) \ln\left(\frac{I_{sc} - I_{mp}}{I_{sc}}\right)}$$

420 Different results obtained at case6 in Fig. 15(c), where a faulty PV string occurred in each PV  
 421 configuration. The value of  $V_{te}$  for the SP, TCT and BL is increased because the value of the  $I_{sc}$  and  $I_{mp}$  is  
 422 decreased:

$$423 \quad V_{te} \uparrow = \frac{(2V_{mp} \downarrow - V_{oc} \downarrow)(I_{sc} \downarrow - I_{mp} \downarrow)}{I_{mp} \downarrow - (I_{sc} \downarrow - I_{mp} \downarrow) \ln\left(\frac{I_{sc} \downarrow - I_{mp} \downarrow}{I_{sc} \downarrow}\right)} \text{ denominator is decreasing more than numerator}$$

424 Similar results obtained for the estimated  $V_{te}$  in the column-level faulty PV conditions as shown in Fig  
 425 15(d). The main findings of this section can be listed as the following:

- 426
- When the number of faulty PV modules in increasing the estimated  $R_s$  is decreasing in S, SP TCT  
 427 and BL configurations.
  - The FF for the S and P configurations among all faulty PV conditions remains at 73.2%.
  - The estimated value of  $V_{te}$  for S, SP, TCT and BL configurations is decreased while increasing  
 429 the number of faulty PV modules. However, in case of the faulty PV string occurred in the PV  
 430 system, the value of the  $V_{te}$  is increased only in SP, TCT and BL configurations.  
 431

432  
433

- P configuration has approximately constant levels of FF and  $V_{te}$  among all tested PV faulty conditions.

Table 10

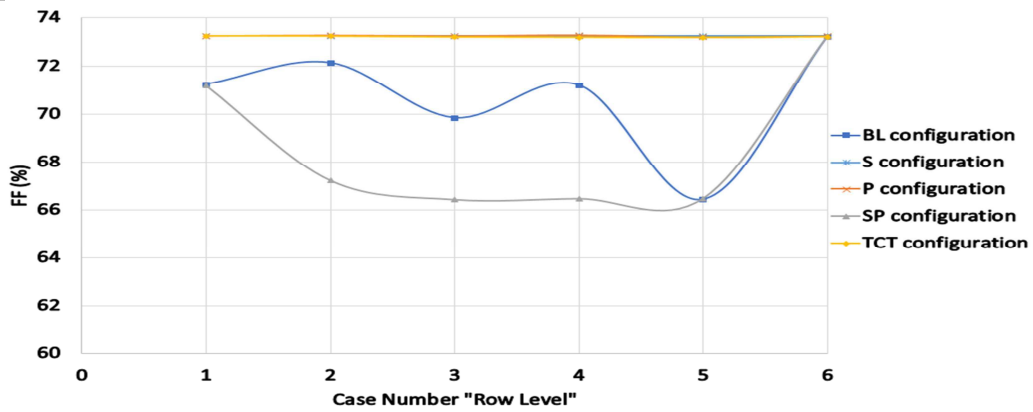
Estimated  $R_s$  for the Multiple Array Configurations, Scenario 3: PV Faulty Conditions, Row Level

Case #	Estimated $R_s$ ( $\Omega$ )				
	S	P	SP	TCT	BL
Case 1	11.57273	0.022096	0.800641	0.631313	0.829876
Case 2	11.08033	0.023095	1.01688	0.505306	0.591541
Case 3	10.58574	0.024196	0.889442	0.379219	0.596659
Case 4	10.08065	0.025408	0.596659	0.253936	0.333778
Case 5	9.581603	0.026748	0.299043	0.128304	0.298151
Case 6	9.077156	0.028226	1.00776	1.00776	1.00776

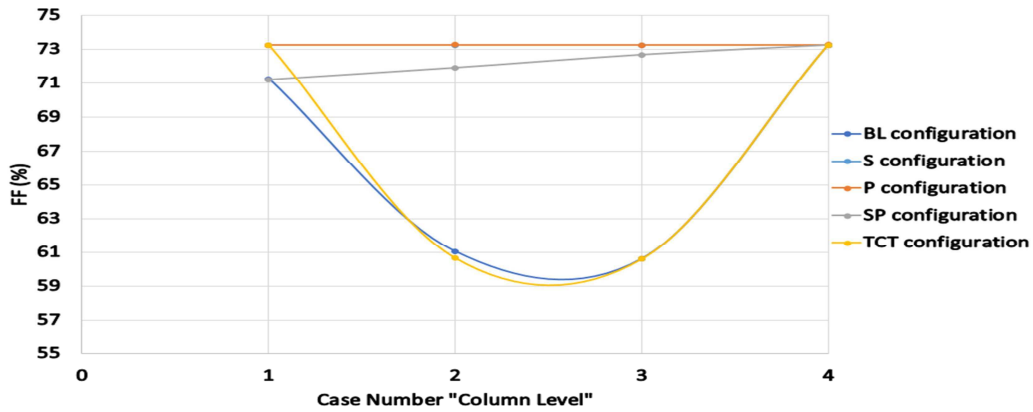
Table 11

Estimated  $R_s$  for the Multiple Array Configurations, Scenario 3: PV Faulty Conditions, Column Level

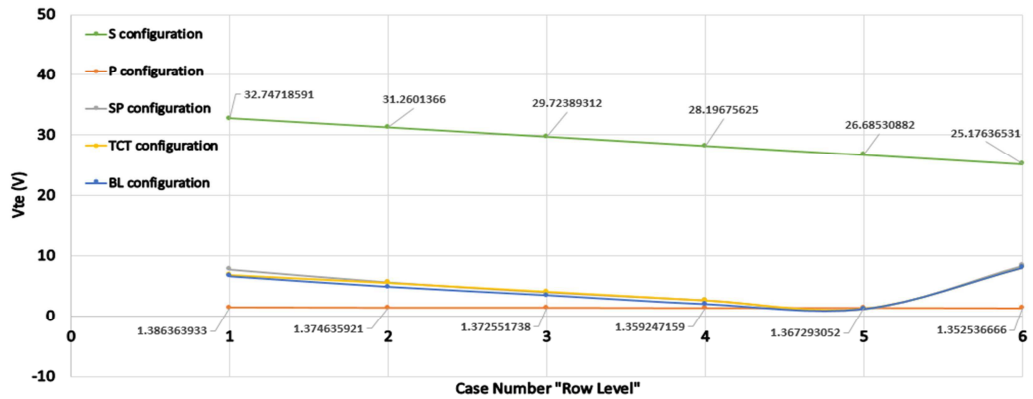
Case #	Estimated $R_s$ ( $\Omega$ )				
	S	P	SP	TCT	BL
Case 1	11.57273	0.022096	0.800641	0.631313	0.829876
Case 2	11.08033	0.023095	0.764526	0.884173	0.913242
Case 3	10.58574	0.024196	0.693481	1.135203	1.135203
Case 4	10.08065	0.025408	0.631313	0.631313	0.631313



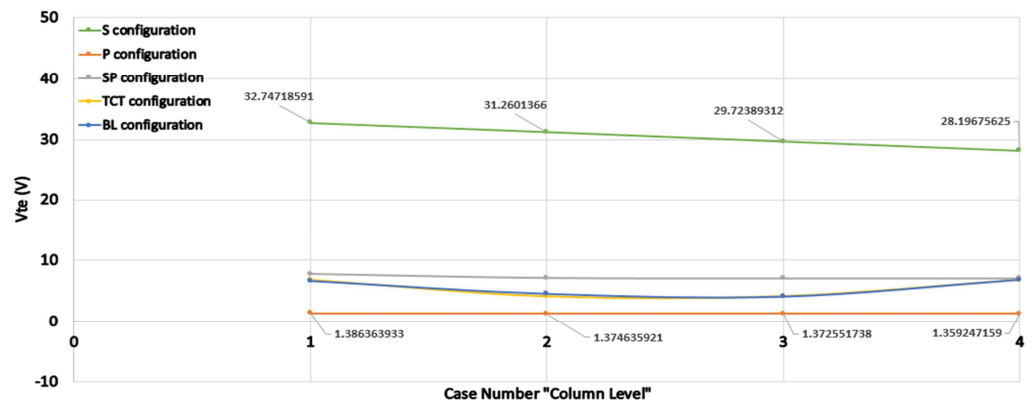
(a)



(b)



(c)



(d)

Fig. 15. FF and  $V_{te}$  Variations for Scenario 3: Faulty PV Conditions. (a) Fill Factor Variations for Row Level PV Faulty Conditions, (b) Fill Factor Variations for Column Level PV Faulty Conditions, (c)  $V_{te}$  Variations for Row Level PV Faulty Conditions, (d)  $V_{te}$  Variations for Column Level PV Faulty Conditions

435 **5. Discussion**

436 In this paper a brief modelling, simulation and data analysis of various partial shading and PV faulty  
 437 modules conditions have been discussed. Multiple diagnostic indicators have been used to compare the  
 438 performance of each PV array configuration such as short circuit current ( $I_{sc}$ ), current at maximum power  
 439 point ( $I_{mpp}$ ), open circuit voltage ( $V_{oc}$ ), voltage at maximum power point ( $V_{mpp}$ ), series resistance ( $R_s$ ), fill  
 440 factor (FF) and thermal voltage ( $V_{te}$ ). Few of these indicators have been demonstrated by F. Belhachat [6].

441 However, the partial shading conditions applied in this paper is not static as shown in [6, 7, 9 and 13],  
 442 which means that the partial shading conditions are either increasing or decreasing among all PV  
 443 modules. Additionally, in order to test the performance of each PV array configuration under faulty PV  
 444 conditions, from 1 to 6 Faulty PV modules have been disconnected in order to compare between each PV  
 445 indicator variations, this scenario has been demonstrated in section 4.3.3. Currently, there are few  
 446 research articles which combines between faulty PV conditions with multiple PV array configurations.  
 447 Therefore, this section is one of the major contribution for this paper.

448 The obtained results of this research can be divided into four main categories:

449 1. PV array configurations under standard test condition (STC):

- 450 • The S, P, SP, TCT and BL configurations provide the same maximum output power.
- 451 • FF for all PV array configurations is approximately equal to 73.2%.
- 452 • New mathematical expressions have been derived for estimating the value of the series  
 453 resistance  $R_s$  across one PV module in all tested PV array configurations.

454 2. PV array configurations under uniform partial shading conditions:

- 455 • P configuration provides the maximum output power when one to five rows or/and one to  
 456 four columns are completely shaded.
- 457 • S, SP, TCT and BL configurations have an increase of the  $R_s$  while increase the uniform  
 458 shading across the PV modules. While P configuration series resistance remains at the  
 459 same value which is approximate to 0.02  $\Omega$ .
- 460 • FF for the S, SP, TCT and BL configurations have a significant drop in its value while  
 461 increasing the uniform partials shading condition applied to a row of PV modules.  
 462 However, the P configuration FF remains at a threshold of 74%.
- 463 • The value of  $V_{te}$  is not a proper indicator for predicting/estimating the change in the  
 464 partial shading conditions for S, SP, TCT and BL since it does not change among all  
 465 tested uniform partial shading conditions.

466 3. PV array configurations under non-uniform partial shading conditions:

- 467 • P configuration provides the maximum output power when one to five rows and/or one to  
 468 four columns are completely shaded. Furthermore, TCT configuration provided the  
 469 second optimum output power among all other PV array configurations.
- 470 • S, SP, TCT and BL configurations have an increase of the  $R_s$  while increase the non-  
 471 uniform shading across the PV modules. While P configuration series resistance remains  
 472 at the same value which is approximate to 0.02  $\Omega$ .
- 473 • SP, TCT and BL configurations proves that when the reduction in the irradiance is greater  
 474 than 2900  $W/m^2$  the estimated value of  $V_{te}$  is always greater than  $V_{te}$  threshold.  
 475 Moreover, S configuration shows that the value of the  $V_{te}$  is greater than  $V_{te}$  threshold if:  
 476 Reduction in irradiance  $\geq 6000 W/m^2$ .

- 479 4. PV array configurations under faulty PV conditions:  
 480 • P configuration provides the maximum output power when one to five PV modules are  
 481 faulty in a row of PV modules and when one to four PV modules are disconnected from a  
 482 column of PV modules in the PV array configuration.  
 483 • The estimation of the  $R_s$  of a single PV module in the PV array configurations can be  
 484 calculated using the following mathematical expression:  
 485  $\bar{S}$  configuration 
$$\frac{R_s \text{ (Obtained from the I-V Curve)}}{24_{(\text{total PV module in the PV array configuration})}}$$
  
 486  
 487 P configuration 
$$R_s \text{ (Obtained from the I-V Curve)} \times 24_{(\text{total PV module in the PV array configuration})}$$
  
 488  
 489 SP, TCT and BL configurations 
$$\frac{R_s \text{ (Obtained from the I-V Curve)} \times 4_{(\text{number of PV columns})}}{6_{(\text{number of PV modules in one PV row "PV String" )}}$$
  
 490  
 491  
 492  
 493 m  
 494 ated value of  $V_{te}$  for S, SP, TCT and BL configurations is decreased while increasing the  
 495 number of faulty PV modules. However, in case of faulty PV string occurred in the PV  
 496 system, the value of the  $V_{te}$  is increased only in SP, TCT and BL configurations.  
 497 • The FF for the S and P configurations among all faulty PV conditions remains at 73.2%.  
 498 However, for all other PV configurations the estimated value of the FF is either  
 499 increasing or decreasing.

500 From the obtained results, it is evident that the variations of  $I_{sc}$ ,  $I_{mpp}$ ,  $V_{oc}$ , and  $V_{mpp}$  are not shown. This is  
 501 because the value of these indicators have been widely discussed by many research articles such as [6, 7,  
 502 9 and 13]. However, all listed references does not include the increase or decrease of shading patterns  
 503 among all PV configurations, additionally, there are few of discussions about faulty PV modules in  
 504 multiple PV array configurations.

505 Table 12, 13 and 14 illustrates the variations for all indicators used in this article among all examined  
 506 partial shading and faulty PV conditions in the S, P, SP, TCT and BL PV array configurations. Three  
 507 different symbols are used to show whether the value of the indicator has an “↓” decrease, “↑” increase,  
 508 “–“ no change in its value and ↓↑ decrease or increase in the value of the indicator. A brief discussion of  
 509 the indicators  $R_s$ , FF and  $V_{te}$  are is available in section 4.

510 The S, SP, TCT and BL configurations have always a reduction in the value of  $V_{oc}$  while increasing the  
 511 uniform, non-uniform shading conditions and increasing the number of faulty PV modules. The P  
 512 configuration has a reduction in the  $V_{oc}$  among all shading patterns, however,  $V_{oc}$  remains constant while  
 513 increasing or decreasing the number of faulty PV modules.

514 In most tested conditions, the value of the  $I_{sc}$  has no change for the S, SP, TCT and BL configurations.  
 515 The P configuration proves that the value of  $I_{sc}$  is always decreasing while increasing the uniform, non-  
 516 uniform shading conditions and increasing the number of faulty PV modules.

517 The voltage at maximum power point ( $V_{mpp}$ ) is not a proper indicator for estimating/predicting partial  
 518 shading conditions or/and faulty PV modules in the S, SP, TCT and BL configuration because in each  
 519 tested condition the value of  $V_{mpp}$  is either increased or decreased. However, this comment is not  
 520 applicable for the P configuration because the value of the  $V_{mpp}$  is always decreasing while increasing the  
 521 partial shading conditions applied to the PV plant.

- 522 The last indicator,  $I_{mpp}$  is a proper indicator to estimate/predict partial shading conditions in all examined  
 523 PV array configurations since the value of the indicator is decreasing while increasing shading conditions.  
 524 The value of  $I_{mpp}$  does not change while increasing/decreasing number of faulty PV modules in S, SP,  
 525 TCT and BL configurations. However, it does change significantly for the P configuration.

Table 12  
 Change in the Estimated Indicators on Each PV Array Configuration

Scenario	PV array configurations													
	S							P						
	$I_{sc}$	$I_{mpp}$	$V_{oc}$	$V_{mpp}$	$R_s$	FF	$V_{te}$	$I_{sc}$	$I_{mpp}$	$V_{oc}$	$V_{mpp}$	$R_s$	FF	$V_{te}$
Increasing uniform shading on PV row	-	↓	↓	↓↑	↑	↓	↓↑	↓	↓	↓	↓	-	-	-
Increasing non-uniform shading on PV row	-	↓	↓	↓↑	↑	↓	↓↑	↓	↓	↓	↓	-	-	-
Increasing uniform shading on PV column	-	↓	↓	↓↑	↑	↓↑	↓↑	↓	↓	↓	↓	-	-	-
Increasing non-uniform shading on PV column	-	↓	↓	↓↑	↑	↓	↓	↓	↓	↓	↓	-	-	-
Increasing faulty PV modules in PV row	-	-	↓	↓	↓	-	↓	↓	↓	-	-	↑	-	↓
Increasing faulty PV modules in PV column	-	-	↓	↓	↓	-	↓	↓	↓	-	-	↑	-	↓

Table 13  
 Change in the Estimated Indicators on Each PV Array Configuration

Scenario	PV array configurations													
	SP							TCT						
	$I_{sc}$	$I_{mpp}$	$V_{oc}$	$V_{mpp}$	$R_s$	FF	$V_{te}$	$I_{sc}$	$I_{mpp}$	$V_{oc}$	$V_{mpp}$	$R_s$	FF	$V_{te}$
Increasing uniform shading on PV row	-	↓	↓	↓↑	↑	↓↑	↑	-	↓	↓	↓↑	↑	↓	↓↑
Increasing non-uniform shading on PV row	-	↓	↓	↓↑	↑	↓	↓↑	-	↓	↓	↓↑	↑	↓	↓↑
Increasing uniform shading on PV column	-	↓	↓	↓	↑	-	-	↓	↓	↓	↓↑	↑	-	-
Increasing non-uniform shading on PV column	-	↓	↓	↓	↑	↓	↓↑	↓	↓	↓	↓↑	↑	↓	↓↑
Increasing faulty PV modules in PV row	-	-	↓	↓	↓↑	↓	↓	-	-	↓	↓	↓	-	↓
Increasing faulty PV modules in PV column	-	-	↓	↓	↓	↑	↓	-	-	↓	↓	↓	↓	↓

Table 14  
Change in the Estimated Indicators on Each PV Array Configuration

Scenario	PV array configuration						
	BL						
	$I_{sc}$	$I_{mpp}$	$V_{oc}$	$V_{mpp}$	$R_s$	FF	$V_{te}$
Increasing uniform shading on PV row	-	↓	↓	↓↑	↑	↓	↓↑
Increasing non-uniform shading on PV row	-	↓	↓	↓↑	↑	↓	↓↑
Increasing uniform shading on PV column	↓	↓	↓	↓	↑	-	-
Increasing non-uniform shading on PV column	↓	↓	↓	↓↑	↑	↓	↓↑
Increasing faulty PV modules in PV row	-	-	↓	↓	↓	↓↑	↓
Increasing faulty PV modules in PV column	-	-	↓	↓	↓↑	↓	↓

## 526 6. Conclusion

527 In this paper, multiple PV array configurations including series (S), parallel (P), series-parallel (SP), total-  
528 cross-tied (TCT) and bridge-lined (BL) have been tested under various partial shading and faulty  
529 photovoltaic (PV) conditions. Several indicators such as short circuit current ( $I_{sc}$ ), current at maximum  
530 power point ( $I_{mpp}$ ), open circuit voltage ( $V_{oc}$ ), voltage at maximum power point ( $V_{mpp}$ ), series resistance  
531 ( $R_s$ ), fill factor (FF) and thermal voltage ( $V_{te}$ ) have been used to compare the obtained results from the  
532 partial shading and PV faulty conditions. MATLAB/Simulink software is used to perform the simulation  
533 and data analysis for each examined PV array configuration.

534 The variations for all indicators across all PV array configurations have been reported and compared  
535 briefly. Additionally, new mathematical expressions have been derived to estimate the value of the series  
536 resistance across a single PV module in each PV array configuration under standard test conditions (STC)  
537 and faulty PV modules.

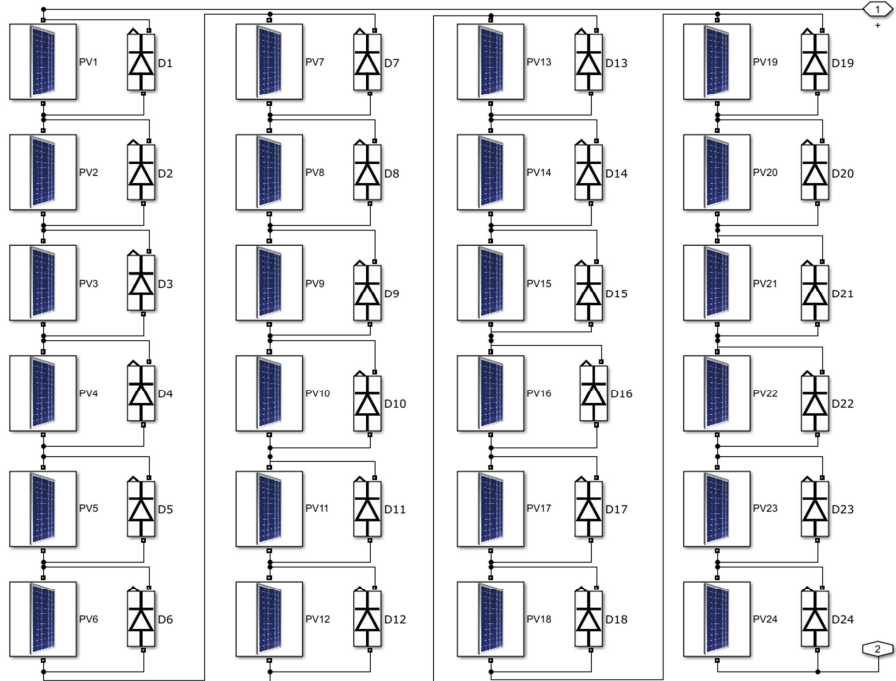
538 Finally, this study gives a useful information on the main parameters that could be used for  
539 estimating/predicting partial shading conditions in all examined PV array configurations. Therefore, the  
540 results obtained from this study could be enhanced by creating a generic algorithm using machine  
541 learning techniques for detecting faulty PV modules in multiple PV array configurations or/and creating  
542 a reconfigurable PV array system to improve the power generation in grid-connected PV (GCPV) plants.

## 543 7. Acknowledgment

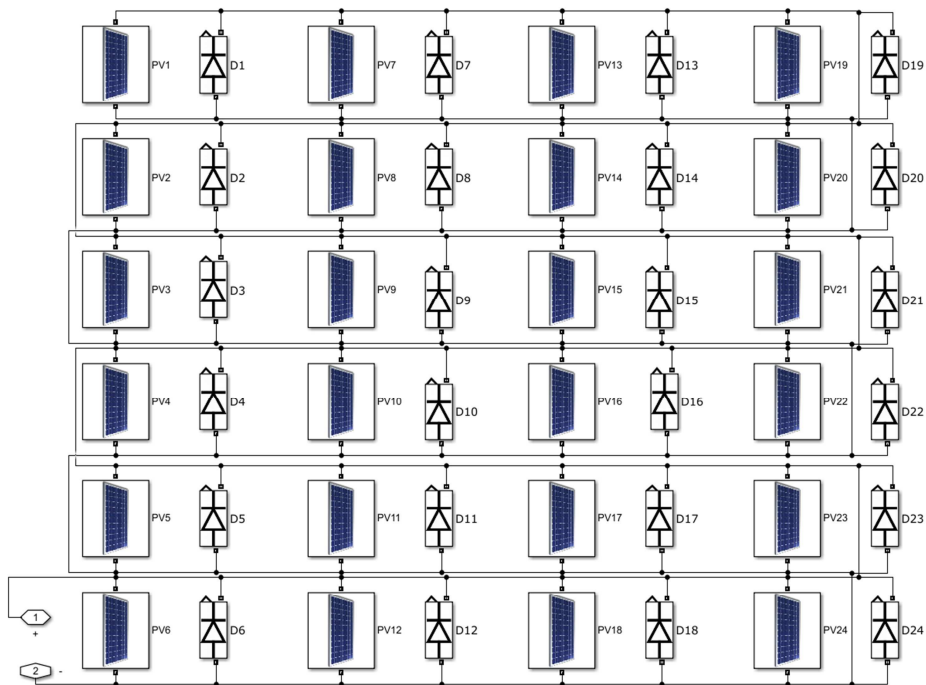
544 The authors would like to acknowledge the financial assistant to the University of Huddersfield,  
545 Engineering and Computing Department.

## 546 Appendix A. MATLAB/Simulink model for the examined PV array configurations.

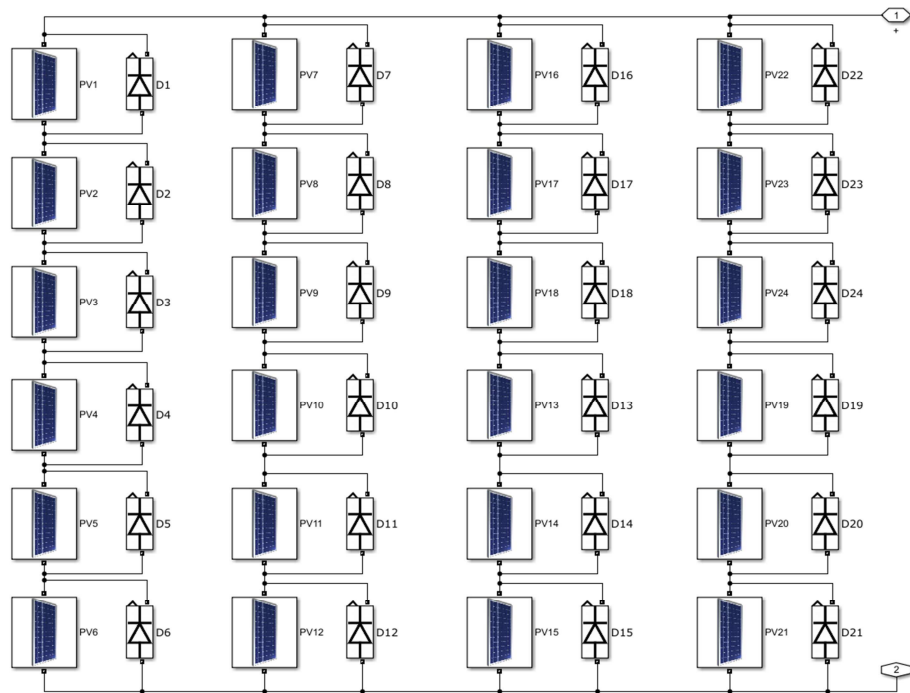
Series (S) Configuration:



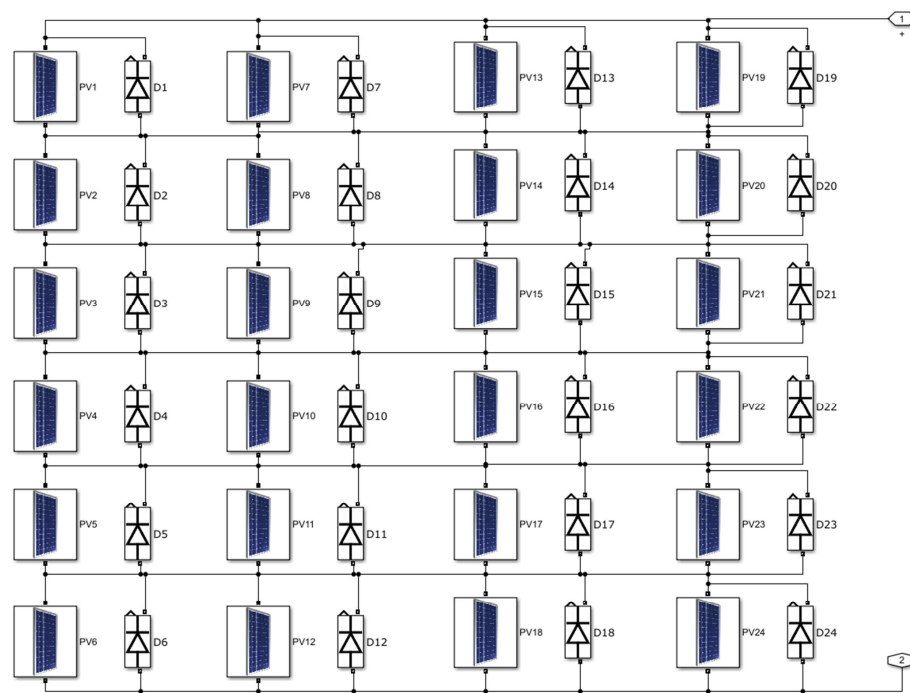
Parallel (P) Configuration:



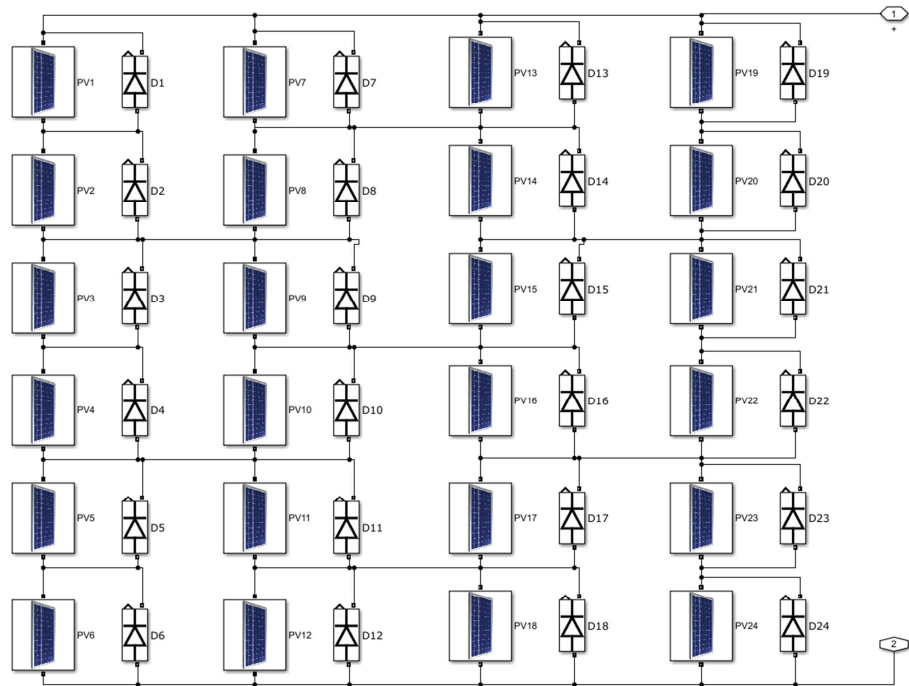
## Series-Parallel (SP) Configuration:



## Total-Cross-Tied (TCT) Configuration:



## Bridge-Linked (BL) Configuration:

547 **References**

- 548 [1] Makrides, G., Zinsser, B., Schubert, M., & Georghiou, G. E. (2014). Performance loss rate of twelve photovoltaic  
549 technologies under field conditions using statistical techniques. *Solar Energy*, *103*, 28-42.
- 550 [2] Lappalainen, K., & Valkealahti, S. (2017). Output power variation of different PV array configurations during irradiance  
551 transitions caused by moving clouds. *Applied Energy*, *190*, 902-910.
- 552 [3] Bai, J., Cao, Y., Hao, Y., Zhang, Z., Liu, S., & Cao, F. (2015). Characteristic output of PV systems under partial shading or  
553 mismatch conditions. *Solar Energy*, *112*, 41-54.
- 554 [4] Di Vincenzo, M. C., & Infield, D. (2013). Detailed PV array model for non-uniform irradiance and its validation against  
555 experimental data. *Solar Energy*, *97*, 314-331.
- 556 [5] Yeung, R. S. C., Chung, H. S. H., Tse, N. C. F., & Chuang, S. T. H. (2017). A global MPPT algorithm for existing PV system  
557 mitigating suboptimal operating conditions. *Solar Energy*, *141*, 145-158.
- 558 [6] Belhachat, F., & Larbes, C. (2015). Modeling, analysis and comparison of solar photovoltaic array configurations under  
559 partial shading conditions. *Solar Energy*, *120*, 399-418.
- 560 [7] Mohammadnejad, S., Khalafi, A., & Ahmadi, S. M. (2016). Mathematical analysis of total-cross-tied photovoltaic array under  
561 partial shading condition and its comparison with other configurations. *Solar Energy*, *133*, 501-511.
- 562 [8] Wang, Y. J., & Hsu, P. C. (2011). An investigation on partial shading of PV modules with different connection configurations  
563 of PV cells. *Energy*, *36*(5), 3069-3078.
- 564 [9] Ramaprabha, R., & Mathur, B. L. (2012). A comprehensive review and analysis of solar photovoltaic array configurations  
565 under partial shaded conditions. *International Journal of Photoenergy*, *2012*.
- 566 [10] Ishaque, K., & Salam, Z. (2013). A review of maximum power point tracking techniques of PV system for uniform  
567 insolation and partial shading condition. *Renewable and Sustainable Energy Reviews*, *19*, 475-488.
- 568 [11] Pareek, S., & Dahiya, R. (2016). Enhanced power generation of partial shaded photovoltaic fields by forecasting the  
569 interconnection of modules. *Energy*, *95*, 561-572.
- 570 [12] Rani, B. I., Ilango, G. S., & Nagamani, C. (2013). Enhanced power generation from PV array under partial shading  
571 conditions by Shade dispersion using Su Do Ku configuration. *IEEE Transactions on sustainable energy*, *4*(3), 594-601.

- 572 [13] Potnuru, S. R., Pattabiraman, D., Ganesan, S. I., & Chilakapati, N. (2015). Positioning of PV panels for reduction in line  
573 losses and mismatch losses in PV array. *Renewable Energy*, 78, 264-275.
- 574 [14] Chong, B. V. P., & Zhang, L. (2013). Controller design for integrated PV-converter modules under partial shading  
575 conditions. *Solar Energy*, 92, 123-138.
- 576 [15] Sun, D., Ge, B., Peng, F. Z., Haitham, A. R., Bi, D., & Liu, Y. (2012, May). A new grid-connected PV system based on  
577 cascaded H-bridge quasi-Z source inverter. In *Industrial Electronics (ISIE), 2012 IEEE International Symposium on* (pp. 951-  
578 956). IEEE.
- 579 [16] Koutroulis, E., & Blaabjerg, F. (2012). A new technique for tracking the global maximum power point of PV arrays  
580 operating under partial-shading conditions. *IEEE Journal of Photovoltaics*, 2(2), 184-190.
- 581 [17] Deshkar, S. N., Dhale, S. B., Mukherjee, J. S., Babu, T. S., & Rajasekar, N. (2015). Solar PV array reconfiguration under  
582 partial shading conditions for maximum power extraction using genetic algorithm. *Renewable and Sustainable Energy*  
583 *Reviews*, 43, 102-110.
- 584 [18] Dhimish, M., & Holmes, V. (2016). Fault detection algorithm for grid-connected photovoltaic plants. *Solar Energy*, 137,  
585 236-245.
- 586 [19] Dhimish, M., Holmes, V., & Dales, M. (2016, September). Grid-connected PV virtual instrument system (GCPV-VIS) for  
587 detecting photovoltaic failure. In *Environment Friendly Energies and Applications (EFEA), 2016 4th International Symposium*  
588 *on* (pp. 1-6). IEEE.
- 589 [20] Chine, W., Mellit, A., Pavan, A. M., & Kalogirou, S. A. (2014). Fault detection method for grid-connected photovoltaic  
590 plants. *Renewable Energy*, 66, 99-110.
- 591 [21] Chine, W., Mellit, A., Lughi, V., Malek, A., Sulligoi, G., & Pavan, A. M. (2016). A novel fault diagnosis technique for  
592 photovoltaic systems based on artificial neural networks. *Renewable Energy*, 90, 501-512.
- 593 [22] Silvestre, S., da Silva, M. A., Chouder, A., Guasch, D., & Karatepe, E. (2014). New procedure for fault detection in grid  
594 connected PV systems based on the evaluation of current and voltage indicators. *Energy Conversion and Management*, 86, 241-  
595 249.
- 596 [23] McEvoy, A., Castaner, L., & Markvart, T. (2012). *Solar cells: materials, manufacture and operation*. Academic Press.
- 597 [24] Sera, D., Teodorescu, R., & Rodriguez, P. (2007). PV panel model based on datasheet values. Paper presented at the 2392-  
598 2396. doi:10.1109/ISIE.2007.4374981
- 599 [25] Silvestre, S., Boronat, A., & Chouder, A. (2009). Study of bypass diodes configuration on PV modules. *Applied*  
600 *Energy*, 86(9), 1632-1640.
- 601 [26] Sera, D., Teodorescu, R., & Rodriguez, P. (2008, November). Photovoltaic module diagnostics by series resistance  
602 monitoring and temperature and rated power estimation. In *Industrial Electronics, 2008. IECON 2008. 34th Annual Conference*  
603 *of IEEE* (pp. 2195-2199). IEEE.
- 604 [27] Spataru, S., Sera, D., Kerekes, T., & Teodorescu, R. (2015). Diagnostic method for photovoltaic systems based on light I-V  
605 measurements. *Solar Energy*, 119, 29-44.
- 606 [28] Bastidas-Rodríguez, J. D., Franco, E., Petrone, G., Ramos-Paja, C. A., & Spagnuolo, G. (2015). Model-based degradation  
607 analysis of photovoltaic modules through series resistance estimation. *IEEE Transactions on Industrial Electronics*, 62(11),  
608 7256-7265.
- 609 [29] Sera, D., Mathe, L., Kerekes, T., Teodorescu, R., & Rodriguez, P. (2011, November). A low-disturbance diagnostic function  
610 integrated in the PV arrays' MPPT algorithm. In *IECON 2011-37th Annual Conference on IEEE Industrial Electronics*  
611 *Society* (pp. 2456-2460). IEEE.

**Highlights**

- Analysing multiple photovoltaic (PV) array configurations under partial shading and faulty PV conditions.
- Seven Indicators have been examined including  $I_{sc}$ ,  $I_{mpp}$ ,  $V_{oc}$ ,  $V_{mpp}$ ,  $R_s$ , FF and  $V_{te}$ .
- New mathematical calculations for estimating the series resistance across one PV module in a PV array configuration is proposed.